# Effective Properties For Flow In Heterogeneous Porous Media

by
Junlin Zhu

Dissertation submitted to the Faculty of the
Virginia Polytechnic Institute and State University
in partial fulfillment of the requirements for the degree of
Doctor of Philosophy
in
Charles E. Via, Jr. Department of Civil Engineering

APPROVED:

John C. Parker, Chairperson

Chin Y. Kuo, Co-chairperson

Douglas G. Boyer

G. V. Loganathan

Gary C. Pasquarell

November, 1990
Blacksburg, Virginia

# Effective Properties For Flow In Heterogeneous Porous Media

by
Junlin Zhu
John C. Parker, chairperson
Chin Y. Kuo, co-chairperson

## (ABSTRACT)

Modeling of groundwater flow and chemical transport calls for a good characterization of heterogeneity of soil properties. The effects of variabilities of soil properties at local scale on the mean behavior of heterogeneous flows were investigated via Monte Carlo method. Assuming log-normal distribution of conductivity and capillary pressure head being a stochastic process, the mean behavior model defined by effective properties was derived to predict the mean behavior of heterogeneous flows. Effective parameters were evaluated numerically and were parametrized in terms of statistics of randomly distributed soil properties and flow characteristics. Monte Carlo simulations were performed to reveal the mean behaviors of steady unsaturated gravity flows, transient areal source infiltration and transient point source infiltration in heterogeneous porous media. The most important findings include (a) the effective conductivity is between the geometric mean and the arithmetic mean, (b) the effective conductivity is time dependent. The derivation of a mean behavior model and the capability of parametrizing the effective properties make it possible to use current deterministic models to predict the mean behavior with minimum changes in the constitutive relations, specifically adding the dependence on the flow characteristic to the $K$-$S$-$P$ relations. The mean model derived in this study was applied to a field site, good agreement was found between the model prediction and field data.

# Acknowledgments

The author wishes to express his sincere and deep appreciation to the chairperson Dr. Parker and the co-chairperson Dr. Kuo of his committee, who gave guidance, advice and encouragement to this study. Without their support and encouragement, this study would not have been possible.

The author would like to thank Dr. Boyer, Dr. Loganathan and Dr. Pasquarell for serving on his Advisory Committee and their time and effort spent on his behalf, and to thank Dr. Boyer for the initiation of the project and his support during its progress. He also wishes to thank Dr. Mishra, who served on his committee before leaving the university, for his comments and suggestions in the early stages of this study.

Special thanks are offered to my wife, Jiangyan, for her endurance and encouragement.

# Table of Contents

# List of Figures

# List of Tables

# Chapter 1 Introduction

Concerns over groundwater contamination due to surface spills or leaks from underground storage facilities have created a great impetus to develop quantitative models for flow in the unsaturated zone. Although the equations governing unsaturated flow are established, precise modeling of complex geologic systems is still a formidable task. One major factor that contributes to the complexity is the large degree of spatial variability exhibited by natural soil formations. Modeling of groundwater flow and chemical transport calls for a good characterization of such heterogeneity.

## 1.1 Heterogeneity

The movement and distribution of moisture and contaminants in unsaturated soils are complicated phenomena. Mathematical formulations representing local processes at a scale of centimeters have been established. The soil is viewed as homogeneous at this scale with a determinable set of physical properties. However, it is recognized that the small-scale properties vary with spatial location, and that the physical system at the scale of interest is heterogeneous. Studies of geological formations indicate the variable nature of hydraulic conductivity and of other characteristic soil-water functions. This variability can no longer be overlooked, as errors resulting from neglected variability might be larger than those resulting from other assumptions included in groundwater flow models. This suggests that it is unproductive to refine available models unless variability is taken into account (El-Kadi 1984).

Due to porous media heterogeneity at many levels, properties relevant at one scale do not in general translate in a straightforward fashion to other scales. It is useful for purpose of discussion to conceptualize a hierarchy of possible

observation scales as follows:

- micro scale - the scale of individual pores [$10^{-5}\ m\ -10^{-3}\ m$]
- meso scale - the scale of core samples [$10^{-2}\ m\ -10^{-1}\ m$]
- macro scale - the scale of typical simulation grids [$1\ m - 10^{2}\ m$]
- mesa scale - the scale of geologic formation [$>10^{3}\ m$]

For example, permeability (k) - saturation (S) - pressure (P) relations observed at the meso (core) scale represent averaging over the scale of many pores, while those observed at the macro (field) scale represent averaging over the scale of many cores. The averaging process to produce effective medium properties at various scales is thus extremely complicated due to innate variability of geologic media at all scales of observations. Investigations at the micro scale are useful for gaining a conceptual understanding of the underlying physical processes which control behavior at the meso scale, but are generally not of direct practical value for engineering analyses of field problems.

Two phase meso S-P relations are conventionally determined by laboratory analyses on soil or rock cores. Parametric representation of two phase meso scale S-P relations is facilitated by the adoption of various empirical models (e.g., Brooks and Corey, 1964; van Genuchten, 1980 ). Two phase meso scale k-S relations may be determined from direct measurements on soil cores, but are often estimated from S-P data based on simple conceptual relationships between capillary pressure and effective flow channel diameter (e.g., Mualem, 1976). Owing to the interdependence of grain size and pore size distributions of unconsolidated porous media, meso scale k-S-P relations are influenced by particle size distribution and a number of methods have been proposed for estimating k-S-P relations from grain size distribution data. (e.g., Arya and Paris, 1981; Haverkamp and Parlance, 1986; Mishra *et al.*, 1988)

Similar to meso analyses, macro and mesa scale systems are viewed as a porous medium. Local properties may differ significantly. One approach to deal with soil heterogeneity would be to construct a detailed deterministic model

which represents the actual variability. However, this degree of resolution would require enormous computational resources, and would be impractical in terms of the amount of data required to define the system. A stochastic approach may be used to attack the problem of variability in soil water properties. In the stochastic approach, uncertainty in the model prediction is defined by assuming that the flow domain is a collection of multiple samples derived from an underlying stochastic process.

## 1.2. Literature Review

A review of the literature indicates that, in general, both deterministic and stochastic approaches have been used to study the problem of heterogeneity. In the deterministic approach, parameters defining the soil water hydraulic properties are assumed to vary in space in a pre-defined manner. The sensitivity analysis approach can be used to assess the response of a model to disturbances of input parameters. This approach identifies the tolerances within which the aquifer or flow parameters might change without affecting significantly the model results. A solution is obtained by repeating the simulation, using different sets of values for the parameter of interest (Bathala *et al.*, 1980). Other approaches in estimating the parameters of the flow equation, known as the inverse problem, can be found in the literature.

In the stochastic approach, the flow domain is assumed to be a collection of multiple samples from a specific distribution. The flow is then solved to define the distribution or at least the first few moments of output variables. Depending on different mathematical approaches, there are several techniques available for stochastic analysis of groundwater flow, for example, spectral analysis, Monte-Carlo simulations, embedding matrix, analogy with wave propagation in random fields, derived distributions, and finite-order analysis (El-Kadi, 1984). The objective of these approaches (except for Monte-Carlo simulations and derived distributions), is to derive the moments, usually up to order 2 (means and variances or covariances) of the output variables from those of input parameters. The derivations are performed by perturbing the governing equations and the solution is obtained in the wave number domain by spectral

analysis (Mantoglou *et al.* 1987). Finite order analysis, similar to perturbation methods, consists of Taylor expansion of solutions of the governing flow equation around the expected values of the parameters and the independent variables ( Dettinger and Wilson 1981).

The embedding matrix approach (Dagan, 1982) consists of discrete homogeneous blocks, of different conductivity and size, which are set at random and independently in space. The calculations are based on writing the governing equations (mass and momentum conservation) for each block and the matching conditions between blocks. Because of the difficulties encountered in the exact treatment, the perturbation approach may be used for the solution. In the derived distributions method and the Monte-Carlo method, the objective is not the derivation of the moments but rather the entire probability distribution of output variables. The Monte-Carlo simulations are based on the repetitive solution of a large number of deterministic flow problems, each time with a different set of generated parameters. Each set is assumed to be an equally probable representation of the actual set. The results are then analyzed statistically to define the distributions of model output. The solution of the deterministic problem can be obtained analytically or numerically.

In the deterministic approach, spatial variability is avoided by implicit averaging of the governing flow equations over the flow domain, thus allowing the use of average input parameters. The validity of this approach can be tested by application of the effective-parameter concept. Using this concept, one tries to replace a medium that exhibits spatial variability by a medium with a single effective set of parameters, while preserving the hydraulic behavior of the original medium.

The scaling-up of constitutive relations from the meso scale to the macro scale is complicated by large scale spatial variations in porous medium properties which precludes the use of simple averaging rules. Moreover it is necessary to treat spatial variability within the context of a stochastic methodology since a full deterministic description of heterogeneous geologic

media is for practical purposes impossible. Several methods have been presented in the literature for generating spatially distributed correlated parameter fields as input to stochastic simulation models (e.g., Journel and Huijbregts, 1978; Luster, 1985; Mantoglou and Wilson, 1982). Applications of these techniques to subsurface flow problems have been generally restricted to the generation of log-normally distributed permeability and/or normally distributed porosity fields with prescribed covariance structures. For unsaturated flow in heterogeneous porous media, it is necessary to generate a distributed field of k-S-P relations. Previous workers (e.g.,Yeh *et al.,* 1985a; Mantoglou and Gelhar, 1987a; Gutjahr *et al.,* 1987) have used simple parametric models to represent the constitutive relations and assumed that parameters of such models can be treated as stationary random processes.

The behavior of effective medium properties for unsaturated flow in heterogeneous porous media has been investigated using both analytical and numerical methods. Yeh *et al.* (1985a,b,c) and Mantoglou and Gelhar (1987a,b,c) have used spectral representation techniques to solve perturbation approximations of the governing stochastic differential equations. They obtained expressions for macro scale properties for two phase air-water flow (Richard's equation) in terms of the mean, variance and covariance of meso scale hydraulic model parameters.

## 1.3. Objectives of Study

The characteristics of meso scale properties are still relevant, but knowledge of the full details of local phenomena is not of concern. Rather the aggregated contribution or the mean behavior of the many local phenomena is important, so the effects on the mean behavior of large scale flow by the local scale properties characterized by their means and covariances are important.

The objective of the study is to investigate the relationship between large-scale effective unsaturated flow parameters, local-scale spatially variable

soil properties and mean flow characteristics using a hybrid perturbation - Monte-Carlo simulation methodology. Random fields of unsaturated flow parameters will be generated from the statistics of grain size data assuming that the variability in soil hydraulic properties is principally due to the variability in local particle sizes. Expressions for effective properties will be derived from perturbation approximations of the governing equations for unsaturated flow. Numerical simulations of transient flow will be conducted to evaluate suitable parametrized forms for the effective properties.

The specific objectives of the study are: (1) To develop a methodology for determining effective macro scale two phase k-S-P relations, (2) To evaluate and parametrize the dependence of effective parameters on soil properties and flow characteristics, (3) To demonstrate the methodology by application to a specific field site.

# Chapter 2 Effective Properties

## 2.1 Background

A widespread problem of groundwater modeling is that of determining the macro-scale behavior of a medium which exhibits microscopic or small scale heterogeneity. It is often convenient to treat heterogeneous soils as if they were samples drawn at random from a population (or ensemble). This approach allows both spatial variability and prediction uncertainty to be analyzed with tools of probability and Monte Carlo simulations.

Bayesian estimation theory establishes a systematic framework for deriving predictions with desirable properties (Schweppe, 1973). This theory may be used, for example, to show that the ensemble mean of capillary pressure head (the primary variable of the governing equation) is the minimum variance unbiased estimate of the actual distribution with finite moments (Jazwinski, 1978). The ensemble variance is a useful measure of the uncertainty associated with this estimate, particularly if the capillary pressure head is normally distributed.

Similar to small scale analysis, large natural systems are viewed as a porous medium. However, it is recognized that the small-scale properties (still considered locally homogeneous and determinable by measurement or observation) vary with spatial location, and that the physical system at the scale of interest should account for the contributions of the small-scale fluctuations.

The contribution of local phenomena in a bulk manner to the nature of flow

and transport in the soil system at larger scales of interest, and the effect of spatial and temporal variability in local properties and local states to the bulk character of water and solute transport are major concerns of studies of heterogeneous flow.

The concept of equivalent parameter values in reproducing the effects of soil spatial variability in current physically based models is of fundamental importance. The main goal is to characterize the large scale or mean behavior by means of equations from which the small scale variation has been eliminated. Sometimes when this goal is achieved, the mean behavior is governed by equations of exactly the same form as those which govern the small scale behavior, but with constant or varying coefficients instead of coefficients which vary on the small scale. Current hydraulic practice assumes that large scale heterogeneity can be lumped into effective parameter values. If such equivalent properties cannot be found to represent the real heterogeneous system, then physically based models have limited practical value.

A variety of methods have been employed to analyze problems of the kind mentioned above. Generally they employ some kind of averaging of the meso or small scale field variables to obtain the effective macroscopic or large scale field variables. Sometimes it is spatial averaging, sometimes stochastic averaging, i.e., averaging over an ensemble of realizations of the meso configuration.

The results of Monte Carlo simulations by Warren and Price (1961), on steady-state groundwater flow, led them to suggest that the geometric mean $K_g$ is capable of representing the non-uniform systems. Freeze (1975) disputed these claims in his analysis of transient one-dimensional saturated flow and concluded that, under such conditions, an equivalent uniform medium is undefinable.

Using analytical expressions, Gutjhar *et al.* (1978) and Dagan (1979) and Bresler and Dagan (1983) demonstrated that effective parameters may only be

meaningful under certain restrictive conditions such as steady flow. Difficulties in selecting an equivalent porous medium under conditions of unsteady vertical infiltration was also reported in the work by Russo and Bresler (1981).

Yeh *et al.* (1985) presented analytical expressions for the effective conductivity of three-dimensional steady unsaturated flow. For soils of low variability, $K_g$ appeared to be a suitable equivalent parameter. Large values of conductivity, however, were found to be appropriate for fields of greater heterogeneity. The findings of Yeh *et al.* thus complemented the earlier conclusions of Dagan (1979) with respect to saturated groundwater movement.

In a Monte Carlo analysis of the drainage of an unconfined aquifer, using a two-dimensional saturated flow approximation, El-Kadi and Brustsaert (1985) noted that the effective hydraulic conductivity was a function of time. For small times, using geometric mean as an equivalent parameter, the outflow of the aquifer was consistently underestimated, although $K_g$ was found to be suitable for larger times. Variability of effective parameters for unsaturated flow has been suggested by Dagan (1982) using analytical expression resulting from perturbation analysis.

Findings of several previous studies of effective conductivities $K_{ef}$ are listed in the following (Binley *et al.*, 1989).

| Source | Flow System | Effective Conductivity |
|---|---|---|
| Gardwell *et al.* and Parson[1945] | 2D steady saturated | $K_{ef} = K_g$ |
| Gutjhar *et al.* [1978] | 2D steady saturated | $K_{ef} = K_g$ |
| Dagan [1979] | 3D steady saturated | $K_{ef} > K_g$ |
| | 2D steady saturated | $K_{ef} = K_g$ |
| Yeh *et al.* [1985] | 3D steady unsaturated | $K_{ef} > K_g$ |
| Freeze [1975] | 3D transient saturated | NO |
| Russo and Bresler [1981] | 1D transient unsaturated | NO |
| Bresler and Dagan [1983] | 1D transient unsaturated | NO |
| El-Kadi and Brutsaert[1981] | 2D transient unsaturated | $K_{ef} = K_g$(at big times) |

Binley *et al.* used the following expression for the effective conductivity

$$K_{ef} = K_g \, exp\left(\frac{p\sigma^2}{2}\right)$$

where

$\sigma^2$ = variance of $ln(K_s)$

$K_s$ = saturated conductivity

$p$ = scaling parameter

Values of $p$ equal to -1, 0, 1 result in $K_{ef}$ being equal to the harmonic, geometric and arithmetic means, respectively. For most cases in their studies, the effective conductivities are greater than the geometric means of the sample distributions.

## 2.2. Derivation of Effective Conductivity and Capacity

### 2.2.1. Governing Equation

For water flow under unsaturated conditions, the point variables of interest are the specific flux $q$, the piezometric pressure head $H$, specific water capacity $C$ and the conductivity $K$. Water capacity is defined as $C = \frac{d\theta}{dh}$, conductivity is related to permeability through the equation $K = \frac{\kappa g}{\nu}$, where $\kappa$ is the permeability, $\nu$ is the kinematic viscosity, $g$ is the gravitational acceleration, and $q$, $H$, and $K$ are related through the continuity equation

$$-\nabla \cdot q + s = \frac{\partial \theta}{\partial t} = C \frac{\partial H}{\partial t} \tag{2.1}$$

where $\theta$ is volumetric water content, $s$ is a source/sink term. Darcy's law, which is stated here for a single-phase flow,

$$q = -K \nabla H \tag{2.2}$$

The meso scale behavior of transient unsaturated flow in a 2-D vertical domain is given by the Richard's equation

$$C \frac{\partial h}{\partial t} = \frac{\partial}{\partial x}\left(K_x \frac{\partial h}{\partial x}\right) + \frac{\partial}{\partial z}\left(K_z \frac{\partial h}{\partial z} + K_z\right) + s \tag{2.3}$$

where $x$ and $z$ are horizontal and vertical space coordinates, respectively. $H = h + z$, $h$ is the capillary head. $K_x$ and $K_z$ are unsaturated conductivity in $x$ and $z$ directions. At the meso scale, $K_x(h)$, $K_z(h)$ and $C(h)$ are assumed to be described by an empirical parametric model such as van Genuchten's (1980) model. Initial and boundary conditions for Equation(2.3) are

$$h(x,z,0) = h_o(x,z) \qquad \text{for } t = 0 \text{ in } R \qquad (2.4a)$$

$$h(x,z,t) = h_1(x,z,t) \qquad \text{for } t > 0 \text{ on } \Gamma_1 \qquad (2.4b)$$

$$-[K_x \frac{\partial h}{\partial x} n_x + K_z(\frac{\partial h}{\partial z} + 1) n_z]\ n = q_n(t) \qquad \text{for } t > 0 \text{ on } \Gamma_2 \qquad (2.4c)$$

where $R$ denotes the entire domain, $\Gamma_1$ and $\Gamma_2$ are portions of the boundary. Equation(2.4a) describes the initial conditions in terms of the capillary pressure function. Equation(2.4b) describes the boundary $\Gamma_1$ on which Dirichlet or Type-I boundary conditions are applicable. Equation (2.4c) describes the Neuman or Type-II boundary conditions on $\Gamma_2$ where $n$ is the unit normal vector drawn outward from the boundary, $n_x$ and $n_z$ are unit vectors in $x$ and $z$ directions, and $q_n$ is the magnitude of the flux normal to the boundary. Water flux at any point in the flow region is given

$$q_x = -K_x \frac{\partial h}{\partial x} \qquad (2.5a)$$

$$q_z = -K_z(\frac{\partial h}{\partial z} + 1) \qquad (2.5b)$$

It is natural to use a stochastic representation of the local fluctuations of the hydraulic soil properties. The stochastic representation is simply a useful tool of analysis which incorporates the complex spatial variability of the actual soil properties through a practical framework requiring only a limited amount of information (Mantoglou *et al.* 1987). It is assumed that the local soil properties $lnK$, $C$ are realizations of two-dimensional random fields composed of two components. Anticipating a log-normal distribution of hydraulic conductivity, the natural log of the conductivity can be decomposed as $ln(K) = f + f'$, or

$K(h) = K_g(h)e^{f'}$ where $K_g$ is the exponential of the expected value of $f = lnK_g(h)$ (i.e., the geometric mean) and $f'$ represents fluctuation of $ln(K)$ about the mean such that $E\{f'\} = 0$. Likewise, the moisture capacity is decomposed as $C(h) = \overline{C}(h) + C'(h)$, where $\overline{C}$ is mean capacity and $C'$ is the fluctuation with $E\{C'\} = 0$ assuming a symmetric distribution. Assuming that the local soil hydraulic properties $ln(K)$ and $C$ are realizations of two-dimensional, cross-correlated, second-order stationary, statistically isotropic random fields, the local flow Equation(2.3) can then be viewed as a partial differential equation with stochastic parameters. Therefore $h$ is a stochastic process, which may be stated as

$$h = \overline{h} + h' \tag{2.7}$$

it will be assumed that $E\{h'\} = 0$.

Taking the derivatives of Eq.(2.7) and defining $J_i = \frac{\partial h}{\partial x_i}$, $\overline{J}_i = \frac{\partial \overline{h}}{\partial x_i}$ and $J'_i = \frac{\partial h'}{\partial x_i}$ one has

$$J_x = \overline{J}_x + J'_x \tag{2.8a}$$
$$J_z = \overline{J}_z + J'_z \tag{2.8b}$$

where $J_z = \frac{\partial h}{\partial z} + 1$, $\overline{J}_z = \frac{\partial \overline{h}}{\partial z} + 1$, and $J'_z = \frac{\partial h'}{\partial z}$. Since we assumed $E\{h'\} = 0$, it follows that $E\left\{\frac{\partial h'}{\partial x_i}\right\} = 0$, therefore the mean gradient of head is the same as the gradient of mean head (i.e., $E\{\frac{\partial h}{\partial x_i}\} = E\{\frac{\partial \overline{h}}{\partial x_i}\}$).

### 2.2.1 Effective Capacity

The effective water capacity $C_{ef}$ is defined by

$$E\{C\frac{\partial h}{\partial t}\} = C_{ef}\frac{\partial \overline{h}}{\partial t} \tag{2.9}$$

Substituting $C = \overline{C} + C'$ and $h = \overline{h} + h'$ into Equation (2.9) and take the

expectation, the following is obtained

$$\overline{C}\,\frac{\partial \overline{h}}{\partial t} + E\{C'\frac{\partial h'}{\partial t}\} = C_{ef}\,\frac{\partial \overline{h}}{\partial t} \tag{2.10}$$

Solve Equation (2.10) for $C_{ef}$

$$C_{ef} = \frac{\overline{C}\,\frac{\partial \overline{h}}{\partial t} + E\{C'\frac{\partial h'}{\partial t}\}}{\frac{\partial \overline{h}}{\partial t}} \tag{2.11}$$

Assuming the mean head derivative is equal to the derivative of the mean head, the effective capacity is defined as the sum of the mean capacity and the ratio of the covariance over mean head derivative, i.e.

$$C_{ef} = \overline{C} + \frac{E\{C'\frac{\partial h'}{\partial t}\}}{\frac{\partial \overline{h}}{\partial t}} \tag{2.12}$$

### 2.2.2. Effective Conductivity

The effective conductivity is defined such that its product with the mean head gradient yields the expected value of the flux at a point. Under the assumption of ergodicity, the effective conductivity can also be defined such that if flow for a given domain is simulated with the effective conductivity, it would yield the same flux as if it were simulated using the detailed spatial distribution of conductivity in the domain. In an isotropic medium, where the flux and gradient vectors coincide, the effective conductivity can be defined by the ratio

$$K_{ef} = \frac{E\{KJ\}}{E\{J\}} \tag{2.13}$$

Similarly we have $E\{K_x\frac{\partial h}{\partial x}\} = K_{xef}\, E\{\frac{\partial h}{\partial x}\}$, and $E\{K_z(\frac{\partial h}{\partial z}+1)\} = K_{zef}E\{\frac{\partial h}{\partial z}+1\}$ for $x$ and $z$ directions.

Since $J = \overline{J} + J'$ and $E\{x\}E\{y\} = E\{xy\} - E\{(x-\overline{x})(y-\overline{y})\}$, one has

$$\frac{1}{E\{J\}} = \frac{E\{\overline{J} - J'\}}{E\{\overline{J}+J'\}E\{\overline{J}-J'\}} \tag{2.14}$$

or

$$\frac{1}{E\{J\}} = \frac{E\{\overline{J} - J'\}}{E\{(\ \overline{J}+J'\ )(\overline{J}-J')\} - E\{(\overline{J}+J'-\overline{J})((\overline{J}-J'-\overline{J})\}} \tag{2.15}$$

and simplifying Equation (2.15) leads to

$$\frac{1}{E\{J\}} = \frac{E\{\overline{J} - J'\}}{E\{\overline{J}^2\} - E\{J'^2\} + E\{J'^2\}} = \frac{1}{\overline{J}^2}\, E\{\overline{J} - J'\} \tag{2.16}$$

Substituting $K = K_g e^{f'}$ and Equation (2.16) into Equation (2.13) and expanding

$$K_{ef} = \frac{1}{\overline{J}^2}\, E\{KJ\}E\{\overline{J} - J'\} = K_g\Big(\ 1 + \frac{\sigma_{f'}^2}{2} + E\Big\{e^{f'}\frac{J'}{\overline{J}}\Big\}\Big) \tag{2.17}$$

where $\sigma_{f'}^2$ is the variance of log unsaturated conductivity.

The governing equation describing the mean behavior of unsaturated flow in a heterogeneous soil can now be written as

$$C_{ef}\frac{\partial \overline{h}}{\partial t} = \frac{\partial}{\partial x}\,(K_{xef}\frac{\partial \overline{h}}{\partial x}) + \frac{\partial}{\partial z}\,(K_{zef}\frac{\partial \overline{h}}{\partial z} + K_{zef}) + s \tag{2.18}$$

Relation(2.17) shows that $K_{ef}$ is a function of (1) the geometric mean conductivity, (2) the variance of log conductivity, (3) the covariance of log

conductivity and head gradient through $E\left\{e^{f'\frac{J'}{\overline{J}}}\right\}$, and (4) the head and the head gradient. Equations (2.12) and (2.17) also show that the effective water capacity and effective conductivity exhibit added nonlinearity due to dependence on spatial and temporal derivatives of the mean head $\overline{h}$ and mean gradient $\overline{J}$. Yeh *et al.* (1985) and Mantoglou and Gelhar (1987) have used spectral representation techniques to evaluate the expectation of the perturbation terms such as $E\left\{e^{f'\frac{J'}{\overline{J}}}\right\}$ and $E\{C'h'\}$ in order to derive analytical solutions for the effective parameters. A deterministic numerical method will be used here to solve the flow problem defined by Equation(2.3) in conjunction with a Monte-Carlo approach. The objectives of the Monte-Carlo simulations are first to yield mean results and to evaluate the expectation terms in the expressions for effective water capacity and effective conductivity in order to parametrize them in terms of soil spatial variability statistics ($K_g$, $\sigma_{f'}^2$, $\overline{C}$ and $\sigma_C^2$ variance of capacity) and mean flow attributes ($\overline{h}$, $\overline{J}$).

The Monte-Carlo simulation method is probably a powerful method, which requires few assumptions. The principle of the method is simple. For each realization, the input parameters are completely determined and known, (e.g. the van Genuchten model parameters $\alpha, n$, $K_s$ in Equations (3.1) and (3.2)). Thus the flow equation can be solved numerically for each realization, giving the values of dependent variables (e.g. $h$). It is then possible to statistically analyze the ensemble of the calculated solutions, expected value, variance and distribution function for each location.

The main difficulty with the Monte-Carlo simulation method is how to generate the realizations of the input parameters, which will be discussed in the next chapter. A large number of realizations is necessary in order to get meaningful statistics. For the point source infiltration problem, 307 realizations were used. For the transient 1-D flow, considering the ergodicity, enough number of simulations were also made.

# Chapter 3 Generation of Soil Properties

## 3.1 Soil Hydraulic Property Model

Unsaturated soil hydraulic properties are commonly represented by empirical models which define the relationship between wetting fluid conductivity, saturation and capillary pressure. One widely used model is the VG model (van Genuchten 1980). The VG model is defined as

$$S_e = (1 + (\alpha \mid h \mid)^n)^{-m} \qquad h < 0$$

$$S_e = 1 \qquad h > 0 \tag{3.1}$$

$$K = K_s S_e^{1/2} (1 - (1 - S_e^{1/m})^m \ )^2 \tag{3.2}$$

where:

$S_e = \dfrac{\theta - \theta_r}{\theta_s - \theta_r}$ effective saturation

$h$ = capillary head [L]

$\theta$ = volumetric water content

$K$ = hydraulic conductivity [$LT^{-1}$]

$\theta_r$ = residual water content

$K_s$ = saturated water conductivity[$LT^{-1}$]

$\alpha$ = VG model parameter [$L^{-1}$]

$n$ = VG model parameter

$m = 1 - 1/n$

Since soil textual information is more readily available than static or dynamic hydraulic data, it is appealing to estimate soil properties from particle size distribution data. The basic premise of the procedure is that the $\theta$-$h$ relationship reflects an underlying pore-size distribution which can be deduced from particle size distribution (PSD) data using a physico-empirical model.

The method involves dividing the particle size cumulative distribution function (CDF) into a number of fractions, assigning a pore volume and a volumetric water content to each fraction, and then computing a representative pore radius and a corresponding capillary head. The resulting relation between capillary pressure head $h$ and saturation $S$ is then fitted to the VG model to obtain model parameters $\alpha$ and $n$. Mishra *et al.* (1989) suggested the following expression to estimate saturated conductivity:

$$K_s = 6.18 \times 10^4 \theta_s (d_{50})^2 \tag{3.3}$$

where:

$K_s$ = saturated water conductivity $(cm/hour)$

$d_{50} = exp[\mu_{ln(d)}]$ = median particle diameter $(cm)$

$\mu_{ln(d)}$ = mean of natural logarithm of particle diameter

### 3.2 Moving Average Method

Stochastic studies of unsaturated flow which use numerical methods require procedures for generating spatially variable soil hydraulic properties over a discretized grid. The representation of heterogeneity involves specifying the variability of the nonlinear functional relations between capillary pressure, water content and water conductivity in the flow domain. Commonly used procedures in subsurface hydrology include the nearest-neighborhood approach (Smith and Freeze, 1979; Anderson and Shapiro, 1983; Hopmans *et al.* 1988), a technique based on sampling from the spectral domain (Mejia and Rodriguez-Iturbe, 1974; El-Kadi, 1987), the turning-bands method (Mantoglou and Wilson, 1982; Ababou and Gelhar, 1988), and application of the Fast Fourier Transform (Gutjahr *et al.*, 1987).

In order to represent spatial variations in meso scale constitutive relations in a discretized two dimensional domain, the procedure developed by Mishra *et al.* (1989) was applied to generate distributed parameter fields of meso

scale k-S-P relations varying from block to block in the flow domain. Instead of using statistics of hydraulic properties as input to a random field generator, the primary distributed variables are porosity and local particle size distribution (PSD) moments. These are converted to distributed soil hydraulic functions using a physically based model which assumes water retention and hydraulic conductivity may be predicted from the soil pore size distribution which can in turn be inferred from PSD data and porosity. One important advantage of generating hydraulic properties (i.e., $\alpha$, $n$ and $K_s$) directly from particle size distribution data is that it gives correlations among the parameters.

The moving average method (Matern 1986) is used for generating spatially correlated fields of the mean $\mu_{ln(d)}$ and standard deviation $\sigma_{ln(d)}$ of the natural logarithm of the particle diameter $d$.

This procedure is conceptually simple and produces an isotropic Gaussian distribution which can be characterized by a circular semi-variogram in two dimensions

$$\gamma(\chi) = \sigma^2\left\{1 - \frac{2}{\pi}Cos^{-1}\left(\frac{\chi}{\lambda}\right) + \frac{2\chi}{\pi\lambda}\sqrt{1-\frac{\chi^2}{\lambda^2}}\right\} \tag{3.4}$$

where $\sigma^2$ is the sample variance, $\chi = \sqrt{x^2+y^2}$ and $x$ and $y$ are spatial coordinates. Note that when $\chi > \lambda$, the semi-variance, $\gamma$, equals the sample variance. The moving average technique can be briefly described as follows:

(a) Extend the simulation grid in each dimension by $\lambda$, and generate a set of uniform random numbers, $r(u)$, between 0 and 1 over the entire augmented grid.

(b) Attribute to each node, $s$, in the simulation grid, a value, $p(s)$, equal to the sum of all $r(u)$ located inside a circle of diameter, $\lambda$, centered at $s$.

(c) Standardize the resulting realization, $p(s)$, to a mean of zero and a variance of one, and then scale using the desired mean and variance. This

produces the required Gaussian autocorrelated distribution, $z(s)$.

After $\mu_{ln(d)}$ and $\sigma_{ln(d)}$ are generated at each point in the simulation grid, the local particle size distribution is computed from these two moments using a a polynomial approximation as given in Equation 6.229 of Abramowitz and Stegun (1965). Distributed porosity fields are also generated using the moving average procedure, assuming porosity to be normally distributed and second-order stationary with a correlation structure described by a circular semi-variogaram.

### 3.3 Derivation of Soil Properties from Particle Size Distribution

As direct measurement of hydraulic conductivity and air-water saturation-pressure (S-P) relationships on a large number of cores will be impractical in most situations, using particle size distribution (PSD) data to predict meso scale parameters is an attractive alternative. The rationale for such a procedure is that the particle size distribution exerts a control over the pore size distribution, which in turn is related to the saturation-capillary head relationship. The use of PSD data is appealing from a practical standpoint since it is easily measurable in the laboratory or can be estimated, albeit with some loss of accuracy, from drill logs and/or geophysical survey data. It is assumed that the PSD for a given meso scale location (i.e., core) can be described by a log-normal probability distribution function (PDF) and hence is completely described by the mean, $\mu_{ln(d)}$ and standard deviation $\sigma_{ln(d)}$ of the natural logarithm of the particle diameter $d$.

Calculation of soil water retention relations from particle size distribution data employs the method of Arya and Paris (1981) as implemented by Mishra *et. al.* (1989) which involves dividing the particle size cumulative distribution function into a number of fractions, assigning a pore volume and a volumetric water content to each fraction, and then computing a representative pore radius and a corresponding capillary head. The $\theta(h)$ function is represented by fitting generated $\theta - h$ data to the parametric model of van Genuchten model

for the three unknown parameters ($\alpha, n$ and $\theta_r$). The saturated water content (porosity) is assumed to be known independently. The unknown model parameters are estimated by a nonlinear regression procedure which seeks to minimize

$$\Psi = \sum_i \left\{ \widetilde{\theta}\,(h_i; \alpha, n, \theta_r) - \theta(h_i) \right\}^2 \tag{3.5}$$

where

$\widetilde{\theta}$ = water content predicted by VG model

$\theta$ = water content generated by AP (Arya and Paris, 1981) model

# Chapter 4 Numerical Method

Transient flow in a heterogeneous unsaturated medium cannot be evaluated analytically. Several numerical methods are available to solve the problem (e.g., finite difference, finite element, boundary element methods). The Galerkin finite element method is chosen in this study. The model used in this study was verified with laboratory experiments (Kuo *et al.*, 1989). The advantage of using the finite element method includes better computational efficiency, the ability to accommodate irregular domains and to produce the derivative by-products such as fluxes at Type I boundaries.

## 4.1 Galerkin Finite Element Formulation

Multiplying Eq.(2.3) with a weighting function $W$ and integrating over an element domain $\Omega^e$, one has

$$0 = \int_{\Omega^e} W\{C\,\frac{\partial h}{\partial t} - \frac{\partial}{\partial x}(K_x\frac{\partial h}{\partial x}) - \frac{\partial}{\partial z}(K_z\frac{\partial h}{\partial z}) - s\}dxdz \tag{4.1}$$

Using Green's theorem on Equation(4.1), it can be written in the variational form as

$$0 = \int_{\Omega^e} \{WC\frac{\partial h}{\partial t} + \frac{\partial W}{\partial x}K_x\frac{\partial h}{\partial x} + \frac{\partial W}{\partial z}K_z\frac{\partial h}{\partial z} + K_z\frac{\partial h}{\partial z} - Ws\}dxdz \; -$$

$$\int_{\Gamma^e} W\{K_x\frac{\partial h}{\partial x}n_x + (K_z\frac{\partial h}{\partial z} + K_z)n_z\}ds \tag{4.2}$$

Where $\Gamma^e$ is the total boundary of the element domain $\Omega^e$. The head $h$ can be

approximated by

$$h(x,z,t) = \sum_{j=1}^{n} h_j(t)\phi_j(x,z) \tag{4.3}$$

where $h_j$ are values of $h$ at time $t$ and at point $(x_i, z_i)$, $\phi_i$ are linear interpolation functions, and $n$ is the number of nodal points in an element.

Substituting Eq.(4.3) and $W = \phi_i$ into Eq.(4.1), one obtains

$$0 = \sum_{j=1}^{n}\Bigg( \Big\{ \int_{\Omega^e} C\phi_i\phi_j dxdz \Big\} \frac{\partial h_j}{\partial t} + \Big\{ \int_{\Omega^e} (K_x \frac{\partial \phi_i}{\partial x}\frac{\partial \phi_j}{\partial x} + K_z \frac{\partial \phi_i}{\partial z}\frac{\partial \phi_j}{\partial z})\, dxdz \Big\} h_j \Bigg)$$

$$- \int_{\Gamma^e} \phi_i\, q_n\, ds + \int_{\Omega^e} K_z \frac{\partial \phi_i}{\partial z} dxdz - \int_{\Omega^e} s\phi_i dxdz \tag{4.4}$$

where

$$q_n = -n_x K_x \frac{\partial h}{\partial x} - n_z\Big(K_z \frac{\partial h}{\partial z} + K_z\Big) \tag{4.5}$$

which is the flux across boundary $\Gamma^e$. The finite element formulation of Eq.(4.1) can be written in matrix form as

$$[M^e]\,\{\dot{h}\} + [K^e]\,\{h\} = \{F^e\} \tag{4.6}$$

where

$$M_{ij}^e = \int_{\Omega^e} C\phi_i\phi_j dxdz \tag{4.7}$$

$$K_{ij}^e = \int_{\Omega^e} \Big\{ K_x \frac{\partial \phi_i}{\partial x}\frac{\partial \phi_j}{\partial x} + K_z \frac{\partial \phi_i}{\partial z}\frac{\partial \phi_j}{\partial z} \Big\}\, dxdz \tag{4.8}$$

$$F_i^e = \int_{\Gamma^e} q_n \phi_i ds - \int_{\Omega^e} K_z \frac{\partial \phi_i}{\partial z} dx dz + \int_{\Omega^e} s \phi_i dx dz \tag{4.9}$$

since quadrilateral elements are used, $i, j = 1,2,3,4, [M^e]$ and $[K^e]$ are $4 \times 4$ matrices and $\{F^e\}$ is a vector of four components.

## 4.2 Isoparametric Elements and Numerical Integration

To facilitate an accurate representation of irregular domains, isoparametric elements are used. However, it is difficult to compute the element coefficient matrices and column vectors directly in terms of the global coordinates $x$ and $z$, which are used to describe the governing equation. This difficulty can be overcome by introducing an invertible transformation between a curvilinear element $\Omega^e$ and a master element $\widehat{\Omega}$ of simple shape that facilitates numerical integration of the element equations. The coordinates in the master elements are chosen to be the natural coordinates $(\xi, \eta)$ such that $-1 \leq (\xi, \eta) \leq 1$. Consider the coordinate transformations:

$$x = \sum_{i=1}^{4} x_i \, \widehat{\phi}_i \, (\xi, \eta) \qquad z = \sum_{i=1}^{4} z_i \, \widehat{\phi}_i \, (\xi, \eta) \qquad h = \sum_{i=1}^{4} h_i \, \widehat{\phi}_i \, (\xi, \eta) \tag{4.10}$$

where the element interpolation functions are in natural coordinates, $h_i$ is the solution at $i$th node of an element, and $(x_i, y_i)$ are the global coordinates of the $i$th node of an element $\Omega^e$.

$$\widehat{\Omega}_1 = \tfrac{1}{4}(1-\xi)(1-\eta) \qquad \widehat{\Omega}_2 = \tfrac{1}{4}(1+\xi)(1-\eta)$$

$$\widehat{\Omega}_3 = \tfrac{1}{4}(1+\xi)(1+\eta) \qquad \widehat{\Omega}_4 = \tfrac{1}{4}(1-\xi)(1+\eta) \tag{4.11}$$

In order of perform element calculations, one must transform functions of $x$ and $z$ to functions of $\xi$ and $\eta$. The coordinate transformation of the integrals should be employed.

Let the Jacobian matrix be defined by

$$[J] = \begin{bmatrix} \frac{\partial x}{\partial \xi} & \frac{\partial z}{\partial \xi} \\ \frac{\partial x}{\partial \eta} & \frac{\partial z}{\partial \eta} \end{bmatrix}$$

and let $[J]^{-1}$ or $[J]^*$ be the inverse of the Jacobian matrix

$$[J]^{-1} = [J]^* = \begin{bmatrix} J_{11}^* & J_{12}^* \\ J_{21}^* & J_{22}^* \end{bmatrix}$$

In Equations (4.7) – (4.9) the integrals are functions of $x$ and $z$. Suppose that the mesh of finite elements is generated by a master element $\widehat{\Omega}$. Using the transformation, the following equation is derived

$$K_{ij}^e = \int_{\widehat{\Omega}} \widehat{K}_x \left(J_{11}^* \frac{\partial \widehat{\phi}_i}{\partial \xi} + J_{12}^* \frac{\partial \widehat{\phi}_i}{\partial \eta}\right)\left(J_{11}^* \frac{\partial \widehat{\phi}_j}{\partial \xi} + J_{12}^* \frac{\partial \widehat{\phi}_j}{\partial \eta}\right) +$$

$$\widehat{K}_z \left(J_{21}^* \frac{\partial \widehat{\phi}_i}{\partial \xi} + J_{22}^* \frac{\partial \widehat{\phi}_i}{\partial \eta}\right)\left(J_{21}^* \frac{\partial \widehat{\phi}_j}{\partial \xi} + J_{22}^* \frac{\partial \widehat{\phi}_j}{\partial \eta}\right) J d\xi d\eta$$

$$= \int_{\widehat{\Omega}} F(\xi,\eta) d\xi d\eta \tag{4.12}$$

Now the integral is defined over a rectangular master element and the quadrature can be presented in the form

$$\int_{\widehat{\Omega}} F(\xi,\eta) d\xi d\eta = \int_{-1}^{1} \left( \int_{-1}^{1} F(\xi,\eta) d\eta \right) d\xi = \sum_{i=1}^{M} \sum_{j=1}^{N} F(\xi_I, \eta_J) W_{ij} \tag{4.13}$$

Where $M$ and $N$ denote the number of the quadrature points in the $\xi$ and $\eta$ directions, $(\xi_I, \eta_J)$ denote the Gauss points, and $W_I$ and $W_J$ denote the corresponding Gauss weights. The mass matrix $M_{ij}$ and force vector $F_j$ are evaluated in the same way. Details involved in the numerical evaluation of the element matrices can be found in Reddy (1984).

### 4.3 Finite Difference Approximation in Time

Finite difference methods are typically used in the approximation of the time derivative. Equation (4.6) is approximated by a weighted difference scheme as

$$\left[\hat{K}^e\right]\left\{h^e\right\}^{k+1} = \left\{\hat{F}^e\right\} \tag{4.14}$$

where

$$\left[\hat{K}^e\right] = \omega\left[K^e\right]^{k+1} + \frac{1}{\Delta t}\left[M^e\right]^{k+1}$$

$$\left\{\hat{F}^e\right\} = \left(\frac{1}{\Delta t}\left[M^e\right]^{k+1} - (1-\omega)\left[K^e\right]^{k+1}\right)\left\{h^e\right\}^k + \left\{F^e\right\}^{k+1} \tag{4.15}$$

in which $\omega$ is a weighting factor while is unity for fully implicit backward difference scheme and 0.5 for a Crank-Nicholson scheme.

### 4.4 Solution Procedure

Based on the inter-element continuity conditions all the element matrices are assembled into the global finite model, which is a system of equations in the form

$$\left[\hat{K}_{ij}\right] \times \left\{h_j^{k+1}\right\} = \left\{F_i^{k+1}\right\} \tag{4.16}$$

This system of equations is solved by Gaussian elimination for values of $h_j^{k+1}$ at time level $k+1$. The nonlinearity (dependency of coefficient matrices on the solution) is solved by an iterative method. This involves making an initial guess and then improving the guess by some iterative process until an error criterion is satisfied. Since some components of vector $\{h_j^{k+1}\}$ are known through Type-I boundary conditions (nodes with specified head), the stiffness matrix $[\widehat{K}_{ij}]$ and the force vector $\{F_i^{k+1}\}$ need to be changed accordingly.

If the flux across some part of the boundary is known, it is converted to a nodal value first, then added to the final force vector $\{F_i^{k+1}\}$. If a point source or sink is located at a node, it can be added directly to corresponding component of the force vector $\{F_i^{k+1}\}$. If it is located inside an element, the source or sink should be distributed proportionally to each node of the element.

An iterative scheme based on Newton-Raphson's method was used. Using notation with the summation implied, the difference between the solution and the approximation can be written:

$$K_{ij}\, h_j - F_i = R_i \qquad i,j = 1,2,3 \ldots. n \tag{4.17}$$

where $\{h_j\}$ is the approximation for head in current iteration and $\{R_i\}$ is the residual. To minimize the residual, the improvement $\Delta h_j$ is found through

$$K_{ij}^T\, \Delta h_j = -R_i \tag{4.18}$$

where $K_{ij}^T$ is the tangent or Jacobian matrix which is derived from Equation (4.17) as

$$K_{ij}^T = \frac{\partial R_i}{\partial h_j} = K_{ik}\frac{\partial h_k}{\partial h_j} + \frac{\partial K_{ik}}{\partial h_j} h_k - \frac{\partial F_i}{\partial h_j} \tag{4.19}$$

### 4.1.5 Nodal Flux Computation

After convergence of the iterative solution has been achieved, the fluxes, $q$, are determined by substituting the solution back into the global matrix equation for the rows that correspond to specified nonzero flux nodes.

$$\{q\} = [\widehat{K}]\ \{h\}^{\,k+1} - \{\widehat{F}\} \tag{4.20}$$

# Chapter 5 Monte Carlo Simulations

Monte-Carlo simulations were performed for different flow scenarios in order to numerically evaluate the expectation terms in the expressions for effective parameters, and to parametrize the effective parameters in terms of local scale statistics of soil properties and mean flow attributes.

## 5.1 Unsaturated Steady-State Gravity Flows

Simulations for unsaturated steady-state gravity flow scenarios were performed for three different heterogeneous fields. Table 5.1 shows the statistics of the primary variables ($\mu_{ln(d)}, \sigma_{ln(d)}$) and the generated variables ($\alpha$, $n$, $K_s$) for the three different hypothetical $50 \times 50$ node isotropic porous media used in the unsaturated gravity flow simulations.

The flow system is shown in Figure 5.1. The domain is a $2.5 \times 2.5$ m vertical slice with a $50 \times 50$ mesh. Zero horizontal fluxes are specified on the two vertical sides, and the capillary head is specified at a constant value on the top and bottom sides. For each heterogeneous soil, simulations were performed for 15 different heads, hence water saturations. Because the flow is steady-state and gravity is the only driving force, the average piezometric head gradient $(\frac{\partial h}{\partial z} + 1)$ is 1. In other words, there should be uniformly distributed capillary pressure heads in the system. The moisture is averaged over all the nodes and the flux is averaged over the entire length of either the top or the bottom boundary. The average fluxes across boundaries and the average moisture of the heterogeneous system are compared with results from "equivalent" homogeneous systems.

Figures 5.2-5.7 show the comparisons of the moisture and flux with that predicted using effective parameters. The distributions of the VG parameter show

that $n$ is normally distributed, with the arithmetic mean and geometric mean almost identical. Since saturated conductivity has been shown to be log-normally distributed, the effective macro-scale saturated conductivity $K_s$ is taken to be the geometric mean. By comparing the results from a heterogeneous field with that from an effective homogeneous field, the behavior of two different macro-scale $\alpha$ (arithmetic and geometric means) are shown in Figures 5.2 -5.7. Attempts were also made to use arithmetic mean of $K_s$ and harmonic $\alpha$ as effective parameters. The results (not shown here) indicated that they are not appropriate for effective parameters.

For the saturated and unsaturated steady-state gravity flow simulations, the following observations can be made.

(1) The geometric means of randomly distributed $\alpha$, $n$ and $K_s$ could serve as the effective macro-scale parameters of the VG soil hydraulic model.

(2) For low degrees of saturation, the macro-scale effective parameters tend to underestimate flux; while for high degrees of saturation, they over predict flux. The deviation reaches a maximum in fully saturated soils.

(3) For low degrees of saturation, the effective macro-scale parameters yield very close moisture contents compared to that from the heterogeneous fields. The moisture is overestimated at high saturations.

## 5.2 Transient Flow Simulations for Areal Source

A hypothetical $30 \times 30$ mesh isotropic medium was used for the simulations of infiltration and redistribution. The geometry of the domain and boundary conditions are shown in Figure 5.8. The average initial saturation is 30%. Table 5.2 shows the statistics of the generated random fields.

The evaluation of effective soil hydraulic properties given by Equations (2.12) and (2.17) was carried out as follows. First $\overline{C}$, $K_g$, $\sigma_f^2$ and $E\{e^{f'}\}$ were computed as functions of $h$ from the local $C(h)$ and $K(h)$ functions by direct averaging over the distributions. Simulations were carried out for 30 realizations of the generated heterogeneous porous media by solving Equation (2.3) for the system geometry and boundary conditions shown in Figure 5.8. For a given time step and a particular element, the following terms were calculated by taking averages over the total number of simulations: (a) mean pressure head, $\overline{h}$, and its derivatives, $\frac{\partial \overline{h}}{\partial t}$ and $\frac{\partial \overline{h}}{\partial z}$ , (b) mean water saturation, $\overline{S} = E\{\frac{\theta}{\theta_s}\}$ and (c) the fluctuation terms $E\{e^{f'}\frac{\partial h'}{\partial z}\}$. To ensure a large enough sample size, the ergodicity assumption is used, that is, the probability distribution of a single spatial realization is viewed as that of the ensemble. Since the mean flow is vertical, averaging was also carried out horizontally (over all 30 elements) for each simulation. This averaging procedure yields 30 sets of the above variables for each time step with each set representing averaged values at a given depth. The effective properties defined by Equations (2.12) and (2.17) for the 30 different locations are calculated from the Monte Carlo simulations. For a given time step, 30 following relationships are established.

$$K_{zef}(i) = f(i)\,(K_g, \overline{C},\ \sigma_f^2,\ \overline{h},\ \overline{J}\,) \qquad (i = 1,30)$$

Considering 11 different time steps when all the variables are recorded, there are $11 \times 30$ above relationships for all the Monte Carlo simulations. The expression for the macro scale effective conductivity as function of local scale statistics and flow attributes should be found such that the error between

$K_{ef}$ given by Monte Carlo simulations and that predicted by the expression is minimal. Since the prescribed pressure heads along the top and bottom boundaries are uniform, $K_{xef}$ will not affect the computation of mean flow in the vertical direction - hence $E\{e^{f'}\frac{\partial h'}{\partial x}\}$ was not evaluated. Head contours at t = 1.1 hour for a single realization are shown in Figure 5.8.

When the time derivative of the mean head is large, i.e., $|\frac{\partial \overline{h}}{\partial t}| >> 0$, Equation (2.13) suggests that $C_e \simeq \overline{C}$. On the other hand, when $\frac{\partial \overline{h}}{\partial t} \rightarrow 0$, the mean head is not sensitive to water capacity. Furthermore, numerical evaluation of $E\{C'\frac{\partial h'}{\partial t}\}$ indicated that it is at least one order of magnitude smaller than the mean capacity, $\overline{C}$, at all times. Thus, the effective capacity, $C_{ef}$, was taken to be equal to $\overline{C}$ as a good working approximation.

An examination of the spatial and temporal distribution of this mean fluctuation term indicated that it could be approximated by the following empirical expression

$$E\left\{e^{f'}\frac{J'_z}{\overline{J}_z}\right\} = \frac{\sigma^2_{f'}}{2}\left(\frac{b}{b_m} - 1\right) \tag{5.1}$$

where $b = \frac{\partial \overline{h}}{\partial z} + 1$ and $b_m = Max\,|b|$ where the maximum is taken over the spatial domain at a given time step. Substitution of Equation (5.1) into Equation (2.17) yields the required expression for effective vertical unsaturated conductivity $K_{zef}$

$$K_{zef} = K_g\left(1 + \frac{\sigma^2_{f'}}{2}\frac{b}{b_m}\right) \tag{5.2}$$

The spatial distributions of $\frac{K_{zef}}{K_g}$ computed directly from Equation (2.17) and its approximation given by Equation (5.2) at different time steps are shown in Figure 5.9. The variable exhibits a peak at the wetting front, where $\frac{K_{zef}}{K_g} \simeq 1 + \frac{\sigma^2_{f'}}{2}$, while at some distance from the wetting front $\frac{K_{zef}}{K_g} \simeq 1$. This

indicates that the effective conductivity is approximated by the arithmetic mean at the wetting front and by the geometric mean at distances far from the wetting front. El-Kadi and Brustaert (1985) found that effective conductivity was a function of time. The geometric mean $K_g$ approximated the effective conductivity at large times, but underestimated the outflow from the aquifer for smaller times. Figure 5.9 shows that the effective conductivity is a function of both space and time. When soil becomes saturated at large times or is close to steady-state, $K_g$ can be taken as the effective conductivity, while at initial transient stages, the arithmetic mean is more relevant where the head gradient changes abruptly.

Effective properties, i.e., the $C_{ef}$-$K_{ef}$-$\bar{h}$ relationships, calculated for the synthetic heterogeneous medium using the procedure described above were used to solve Equation (2.18) to predict the response of the "equivalent" homogeneous system for the same initial and boundary conditions used in the base simulations. Mean infiltration rates and head distributions predicted for the actual heterogeneous system using Equation (2.3) and for the equivalent homogeneous system using Equation (2.18) are compared in Figures 5.10 and 5.11.

There is good agreement between the response of the heterogeneous system and that of the equivalent homogeneous system both at short times when flow is highly transient as well as at large times as steady state flow is approached. Attempts to approximate the heterogeneous system with simple geometric mean function $K_g$(h) was insufficient to describe the system behavior accurately (results not shown) indicating that the time dependent nature of the effective properties must be taken into account to obtain an accurate large scale representation of heterogeneous systems.

## 5.3 Optimum Level of Discretization

If unsaturated flow is to be simulated by substituting large-scale effective

parameters for the distributed parameter field in the original mesh, the primary savings in computation will be due to reductions in problem non-linearity and data requirements. To obtain major reductions in computational effort, the total number of grid blocks in the system is reduced. It is therefore useful to investigate the performance of the equivalent homogeneous system as a function of mesh size.

The approach taken in this work for determining an optimum level of discretization involves progressively coarsening the mesh (beginning with the grid at which the effective parameters were computed) to examine how the response of the effective homogeneous system deviates from that of the actual heterogeneous system. The system considered is the same as that shown in Figure 5.8, but with both infiltration and redistribution periods taken into account. Since the effective parameters were determined only from fine-scale simulations of infiltration, adding the redistribution period provides a further test of the applicability and robustness of these effective parameters under a different set of boundary conditions. Four levels of discretization are considered: (1) $30 \times 30$, (2) $25 \times 25$, (3) $20 \times 20$, and (4) $15 \times 15$. For each of these cases, effective parameters determined for simulations of infiltration in the $30 \times 30$ heterogeneous system were used to compute the response of the equivalent homogeneous system with the same initial and boundary conditions.

Figure 5.12 shows the calculated rate of infiltration into the system across the top boundary. The base case corresponds to the response of the $30 \times 30$ heterogeneous system. The response of the equivalent homogeneous systems generally agree well with the base case results, although the infiltration rate tends to be overpredicted when effective parameters are used.

A comparison of the head distributions for the base case and the four equivalent homogeneous systems are shown in Figures 5.13 and 5.14. Pressure profiles at two different times during infiltration ($t \leq 4.7$ hour) and redistribution ($t > 4.7$ hour) are depicted in these figures. There is good agreement between the two sets of responses in general, although the infiltration

data (left) are much better matched than the redistribution data (right) when using effective parameters. The worst agreement occurs consistently for the $15 \times 15$ mesh equivalent homogeneous system, which is easily explained by the higher truncation error associated with the coarse discretization.

Two other interesting observations can be made from the data presented in Figures 5.13 and 5.14. The maximum deviation between the heterogeneous and the equivalent homogeneous system response occurs where the pressure gradients are changing the most. It is apparent that effective parameters are unable to reproduce large gradients at the local scale. The second observation concerns the tendency of the equivalent homogeneous system pressure profiles to converge to the heterogeneous system profile at large redistribution times. This implies that the use of effective properties will be even more appropriate when the effects of a step change at a boundary (i.e., from infiltration to redistribution) have dissipated throughout the system.

## 5.4 Point Source Infiltration Simulations

Monte-Carlo simulations were also preformed for transient infiltration from a point source. The flow domain is a $30 \times 30$ mesh system with generated soil hydraulic properties. Figure 5.15 shows the geometry of the domain and boundary conditions. The domain initially had an average saturation of 50%. Infiltration is induced by specifying pressure head at 2 nodes in the middle of the top boundary. The rest of the top boundary and both sides are zero flux. The statistics of the generated soil properties were shown in Table 5.3.

The evaluation of effective hydraulic properties was carried out in a similar fashion as for 1-D transient flow, except that horizontal averaging was not performed, because the flow is two dimensional. To ensure a large enough sample size, flow was simulated over 307 different realizations of random fields. For a given time step, and for each element in the domain, the following terms were calculated by averaging over the 307 simulations; mean capillary pressure head, $\overline{h}$, mean time derivative $\frac{\partial \overline{h}}{\partial t}$, mean saturation $\overline{S}$, mean water capacity $\overline{C}$, variance of log conductivity $\sigma_f^2$, cross-variance of log conductivity and head gradient, $E\{e^{f'}\frac{\partial h'}{\partial x}\}$ and $E\{e^{f'}\frac{\partial h'}{\partial z}\}$, cross-variance of water capacity and head $E\{C'h'\}$, variance of head, $\sigma_h^2$, and variance of water capacity, $\sigma_c^2$. For a given time step, effective properties defined by Equations (2.12) and (2.17) for all the 900 elements are also calculated.

Figures 5.16 and 5.17 show the saturation distribution and pressure head distributions for a single realization. Contours of saturations at different time steps indicating the movement of moisture are shown in Figures 5.18-5.20.

Following are some observations of the Monte Carlo simulation results.

1. Shown in Figures 5.21-5.26 are contours of the ratio of effective conductivity defined by Equation 2.13 to the geometric mean at different time steps. It is apparent that most contours are between 1.0 and 1.3 which is about $1+\frac{\sigma_{f'}^2}{2}$, indicating most effective conductivities are

between the geometric mean and the arithmetic mean.

2. Comparing the contours of head derivatives with respect to time (Figures 5.39 and 5.41) and contours of head gradients (Figures 5.40 and 5.42), one can see that the ratios reach their peaks in regions where hydraulic gradients are highest (i.e., at the wetting front of the plume, see Figures 5.23 and 5.25). The ratios are close to 1 at some distance away from the wetting front.

3. It should be noted that variance of log conductivity $\sigma^2_{f'}$ at any time step in different meshes do not show any pattern, and the average spatial variance of $\sigma^2_{f'}$ is approximately the same as variance of log saturated conductivity $\sigma^2_{ln(K_s)}$ (see Figures 5.27 and 5.28 for distributions of $\sigma^2_{f'}$ and $\sigma^2_{ln(K_s)}$).

4. The contours of head variance $\sigma^2_h$ (Figure 5.29) shows that it also reaches its peaks at the wetting front, where the hydraulic gradients are high and rates of capillary head changes are also high and positive.

5. Comparing Figures 5.21 and 5.25, one observes that the ratios of effective conductivity over geometric mean decrease slightly with time, which suggests the time dependence of the effective conductivity. At larger times, the head derivative with respect to time decreases.

6. Values of $\frac{C_{ef}}{\overline{C}}$ are close to 1.0 and the standard deviation of water capacity $\sigma_C$ is relatively small, which justifies the use of $\overline{C}$ as a good approximation to $C_{ef}$.

7. Figure 5.38 shows a good agreement in flux between the mean model predictions and the Monte-Carlo simulation results.

Based on the above observations and extensive numerical experiments performed to determine the dependence of the effective conductivity on the static soil properties (statistics of the local soil properties, means and variances)

and dynamic soil properties (flow characteristics, hydraulic gradients, time derivative of head), the following parametric model is proposed:

$$K_{ef} = K_g \left\{ 1 + \frac{\sigma_{f'}^2}{2} J_n \, exp\left(J_t - 1\right) \right\} \tag{5.3}$$

where:

$J_n = J/J_{max}$ is the normalized hydraulic gradient

$J = \sqrt{(\frac{\partial h}{\partial x})^2 + (\frac{\partial h}{\partial z} + 1)^2}$ is the resultant hydraulic gradient

$J_{max} = max(J)$ is the maximum hydraulic gradient at the current time

$J_t = \frac{\frac{\partial h}{\partial t}}{(\frac{\partial h}{\partial t})_{max}}$ is the normalized time derivative of the capillary head

The effective conductivity is a function of capillary pressure head $h$ through $K_g$, the variance of log conductivity, $\sigma_{f'}^2$, which is found to be the same as that of saturated conductivity $\sigma_{ln(K_s)}^2$, the normalized hydraulic gradient and the normalized time derivative of the pressure head. Figures 5.33 and 5.37 show the distribution of $K_{ef}/K_g$ predicted by Equation (5.3).

Due to the dependence on the flow characteristics, the mean model exhibits the anisotropy and hysteresis effects. The discrepancies of wetting fronts observed in Figure 5.31 vs Figure 5.32 and Figure 5.35 vs Figure 5.36 are caused by the anisotropic effects. Results from the "classical" model with single valued effective parameters given by geometric mean parameters (Figure 5.32 and Figure 5.36) underestimated movement at later times. Comparing Figure 5.30 with 5.31 or Figure 5.34 with 5.35, good agreements were found in head distributions between the mean model predictions and the Monte Carlo simulation results. Under the influence of gravity, the plume tends to have a significant vertical movement, resulting in a longer path in the vertical direction, thus creating a relatively higher hydraulic gradient in the lateral direction, and therefore a larger effective conductivity. This dynamic anisotropy

effect would prevent movement of a plume too fast or too far in one direction.

The hysteresis is represented by the exponential term in the effective conductivity equation. As indicated in the simulations for 1-D infiltration and redistribution, the effective conductivity is lower during drying than during wetting. Also, it is found when flow approaches steady-state ( $\frac{\partial h}{\partial t} \rightarrow 0$, usually associated with very small hydraulic gradient $J \rightarrow 0$), the effective conductivity is very close to the geometric mean.

It should be pointed out that the anisotropy and hysteresis effects of the mean behavior model does not result from local scale anisotropy of soil properties, but from the variability of local soil properties, although they are induced by the flow characteristics.

The geometric mean of unsaturated conductivity $K_g$ in Equation(5.3) by definition is

$$K_g = exp\Big(E\Big\{ln\big(K(\alpha, n, K_s; h)\big)\Big\}\Big) \tag{5.4}$$

where $\alpha$, $n$ and $K_s$ are one realization of the randomly distributed VG parameters and $h$ is the capillary pressure head. Comparison was made between $K_g$ averaged from Equation (5.4) and that estimated from VG model with geometric means of the parameters. The results indicated a good approximation of $K_g$ is given by

$$K_g = K_{sg}\, S^{1/2}\Big(1-(1-S^{1/m_g})^{m_g}\Big)^2 \tag{5.5}$$

$$S = [1+\alpha_g\,|\,h\,|^{\,n_g}\,]^{-m_g} \tag{5.6}$$

where

$\alpha_g =$ is the geometric mean of VG parameter $\alpha$

$n_g =$ is the geometric mean of VG parameter $n_g$

$K_{sg} =$ is the geometric mean of saturated conductivity

$m_g = 1 - 1/n_g$

# Chapter 6 Field Application

## 6.1. Simulation Site

The model developed in this study was applied to simulate subsurface runoff in response to a rainfall event at a site located near Beckley, West Virginia. Rainfall data and surface and subsurface runoff data were recorded during the event. Soil moisture contents were measured on the day prior to the rainfall.

Figure 6.1 shows the geometries of plots A-D. Plot A was chosen for the simulation. A barrier was installed along the downstream side of plot to direct the subsurface flow to a measuring device. A vertical transect along the center of Plot A was used as the domain of the 2-D simulation. The bottom boundary was at a depth of 1.1 m where the bed rock materials occurred. Figure 6.2 shows the geometry of the transect. The average slope is 11%.

Soil cores (5.5 cm diameter $\times$4.0 cm height) samples were collected near the site from 10 different locations. At each location, 3 samples were taken at different depths of 20, 50 and 91 cm, respectively. Saturated hydraulic conductivity was measured by a falling head method on each core in the laboratory. Particle size distribution was measured on samples of each core by pipette method. Table 6.1 shows the statistics of the measured saturated conductivities and the conductivities calculated from particle size distribution data, as well as the statistics of VG parameters $\alpha$, $n$ and $\theta_r$ estimated from particle size data.

## 6.2. Boundary and Initial Conditions

Soil moisture data recorded on the day prior to the rainfall event shows a very high degree of saturation. Table 6.2 shows the soil moisture data in

volumetric percent at different locations and depths. A uniform 30 cm capillary pressure head corresponding to 95 percent saturation was specified as the initial conditions for the simulation. A $50 \times 5$ mesh system was used as shown in Figure 6.2. for the finite element simulation. Because the conductiviti es of the rock materials are orders of magnitude smaller than that of the soil above, the bottom boundary of simulation domain is treated as zero-flux boundary when the saturation at the boundary node is not saturated; a zero vertical pressure gradient, i.e. $\frac{\partial h}{\partial z} = 0$, is used when the node at the bottom boundary becomes saturated, in which case flow across the boundary is possible. Side BC of the domain is specified as a zero-flux boundary, and side AD is a seepage face, with a zero flux on the upper part and zero pressure head on the lower section. The location of the seepage face is determined by a trial and error procedure until the mass balance is satisfied. Along the upper surface of the domain DC, during the rainfall, a specified flux equal to the rainfall rate is the boundary condition until the surface becomes saturated, after which zero pressure head is specified. After the rainfall, zero flux is specified on DC.

### 6.3. Results and Discussion

The rainfall data is shown in Figure 6.3. Figure 6.4 shows the comparisons of recorded and simulated subsurface runoff. According to the recorded data, the total amount of runoff including both surface and subsurface runoff is about 142 liters, while the total amount of rainfall received by Plot A is 5,200 liters, which would account for a 5% increase in saturation. In other words about 5,000 liters of water would be detained in the top soil assuming there is no significant flow into the deep soil. The comparison of cumulative surface runoff is shown in Figure 6.5.

A summary of prediction and observation in the following Table 6.3 (in liters).

| | Observed | Predicted |
|---|---|---|
| Rainfall | 5,200 | ------- |
| Sub. Runoff | 135 | 148 |
| Surface Runoff | 7 | 11 |
| Drainage | no data | 72 |
| Storage | no data | 4969 |

The zero vertical pressure gradient could also be applied for the bottom boundary for the whole simulation period, in which case there will be more drainage.

The simulation has proven the effective flow model and the averaging schemes for the soil hydraulic properties developed in this study provide accurate description of subsurface flow.

# Chapter 7 Summary and Conclusions

This study developed a methodology for deriving effective hydraulic properties to simulate mean transient unsaturated flow in heterogeneous porous media. The effective properties in the mean behavior model were evaluated via the Monte Carlo method. This methodology accounts for the existence of local soil property variability and basic nonlinearities of the local governing flow equation. It was assumed that the local soil properties are realizations of two dimensional, second order stationary random fields. The method followed the following steps.

(1) The form of the mean behavior model representation and effective properties for the mean behavior model were derived, assuming log-normal distribution of conductivity and capillary pressure head being a stochastic process.

(2) The van Genuchten soil hydraulic property model was selected to describe the dependence of the unsaturated conductivity $K$ and soil moisture content $\theta$ on capillary pressure head $h$. The randomly distributed soil properties were generated from statistics of particle size distribution data using Arya and Paris model and a moving average method.

(3) Monte-Carlo simulations were performed to reveal the mean behaviors of the steady unsaturated gravity flows, the transient infiltration and the transient two-dimensional flow in heterogeneous porous media. The most important findings include (a) the effective conductivity is between the geometric mean and the arithmetic mean, (b) the effective conductivity is time dependent.

(4) Effective parameters were evaluated numerically and were parametrized in terms of statistics of randomly distributed soil properties and flow characteristics.

(5) Mean behaviors of the above mentioned flow scenarios were simulated and reproduced using the parametrized effective properties in the equivalent homogeneous porous media.

The resulting mean behavior model was expressed in the same form as the local scale partial differential equation, and to predict the mean-behavior rather than the details of a single realization of a random field. The effective parameters of the mean-behavior model do not depend on a single realization of soil properties, but they rather depend on a few parameters describing statistics of local variability (i.e., means and variance). The derivation of a mean behavior model and the capability of parametrizing the effective properties make it possible to use current deterministic models to predict the mean behavior with minimum changes in the constitutive relations, specifically adding the dependence on the flow characteristics to the $K - S - P$ relations.

In their pioneering studies of unsaturated flow in heterogeneous porous media, Montaglou and Gelhar (1987) used an analytical approach to derive the effective properties in the complex integral forms. The anisotropy and hysteresis effects of mean behavior were also found in their analytical studies.

Comparing the results, Figure (5.32), with simple averaging scheme used as effective parameters, for example, geometric means of $K_s$, $\alpha$ and $n$, Figure (5.31) Monte Carlo simulation results, and Figure (5.30) results with proposed effective property model, one could observe that in the MC results and results with effective properties the plume spread more in the horizontal direction, showing the anisotropy effect. One could also recognize the anisotropy effect from the parametrized effective conductivity. It is apparent from Equation (5.3) that the larger the gradient the higher the effective conductivity.

A higher gradient in one direction will give a larger effective

conductivity, the combination of higher gradient and larger conductivity produces faster flow in that direction until the gradient becomes smaller. This anisotropy effect would prevent the flow in one direction becoming too fast. The anisotropy effect of the mean behavior did not resulte from the local scale anisotropy of soil properties, but from the variability of local soil properties.

Monte-Carlo simulations also indicated hysteresis in computed $\frac{K_{ef}}{K_g}$, $\frac{\partial h}{\partial t}$, and $J_n$. On one contour of $J_n$ one could see smaller $\frac{K_{ef}}{K_g}$ at regions where $\frac{\partial h}{\partial t} < 0$. Generally during drying, the effective conductivity is lower than during wetting. This hysteresis effect is included in the parametrized effective property model through the term $J_t$. Like the anisotropy effect, hysteresis in the mean behavior is not caused by local scale hysteresis of porous media, but by the local variability.

It has been demonstrated that unsaturated steady infiltration in heterogeneous media can be simulated by using effective properties. The geometric means of saturated conductivity $K_s$, $\alpha$ and $n$ of VG model can serve as effective parameters. For transient unsaturated flow, the effective properties are functions of both time and space. At larger times when flow reaches steady-state and hydraulic gradients are low, the effective conductivity can be approximated by geometric mean of the heterogeneous soil. At wetting fronts where hydraulic gradients are high, or when time derivative of capillary pressure head is large and positive, the effective conductivity is close to the arithmetic mean. The effective conductivity has been parametrized and tested, and predictions of the mean transient flow in heterogeneous soils agreed well with that of Monte Carlo simulations.

The model was applied to simulate a subsurface runoff in response to a rainfall event for a site located at USDA's Water Conservation Laboratory in Beckley, West Virginia. Soil samples were taken from the site. Soil hydraulic properties were determined by the particle size distribution data via Mishra's method. A good agreement was obtained between the model predicted subsurface runoff and the recorded data.

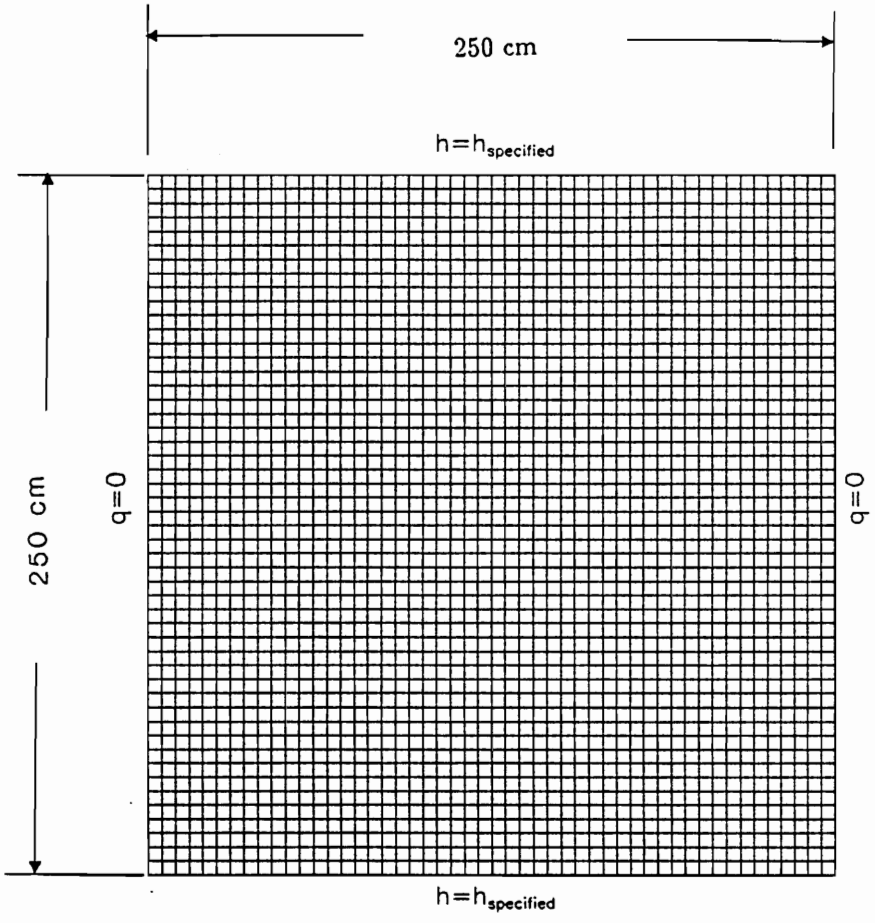


Figure 5.1 Geometry and boundary conditions for steady gravity flow simulations

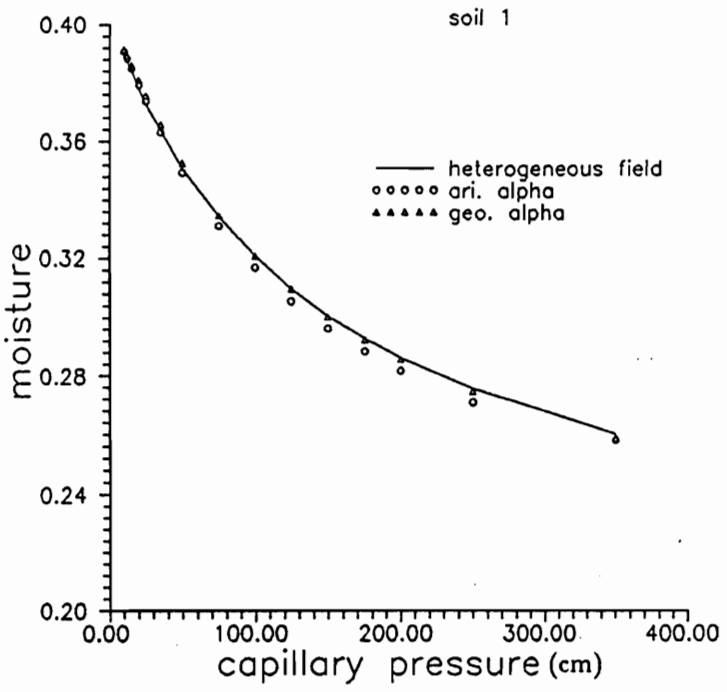


Figure 5.2 Comparison of moisture predicted by using arithmetic, geometric mean properties and by the heterogeneous medium for soil No.1

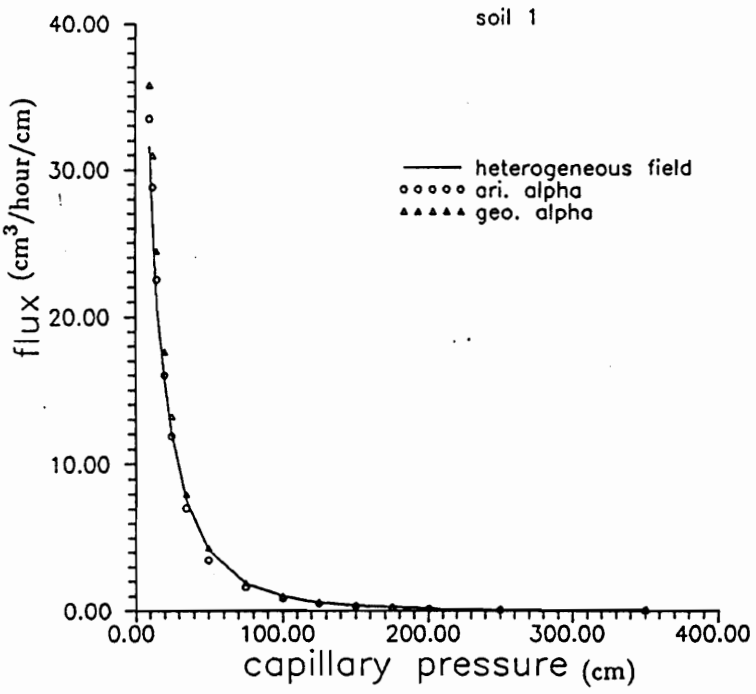


Figure 5.3 Comparison of flux predicted by using arithmetic, geometric mean properties and the heterogeneous medium for soil No.1

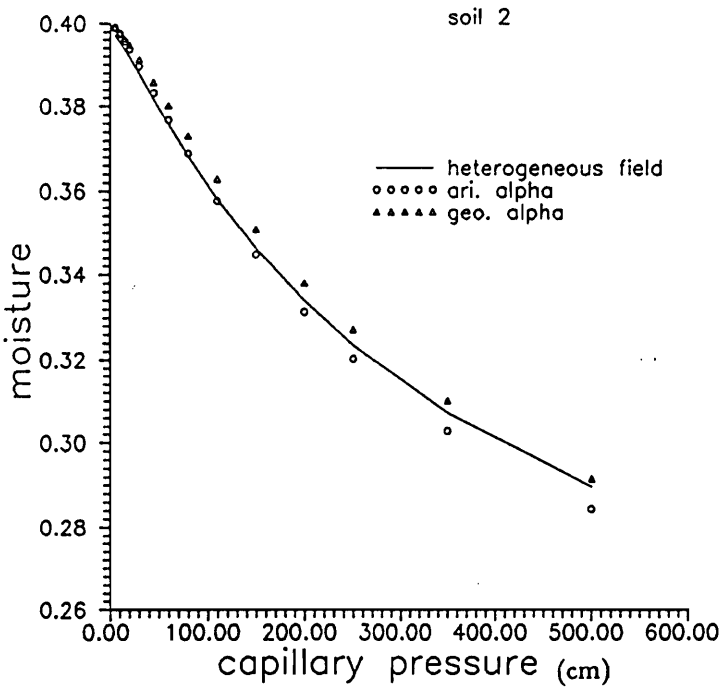


Figure 5.4 Comparison of moisture predicted by using arithmetic, geometric mean properties and the heterogeneous medium for soil No.2

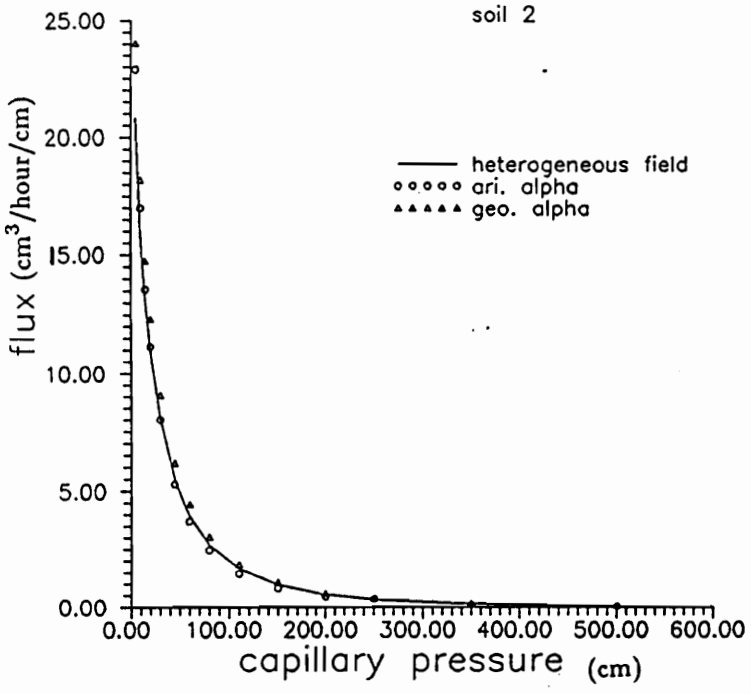


Figure 5.5 Comparison of flux predicted by using arithmetic, geometric mean properties and the heterogeneous medium for soil No.2

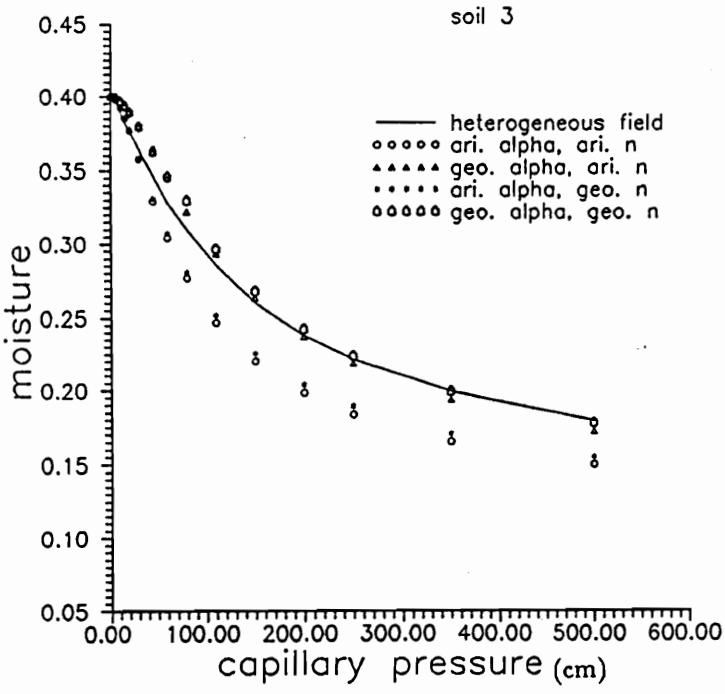


Figure 5.6 Comparison of moisture predicted by using arithmetic, geometric mean properties and the heterogeneous medium for soil No.3

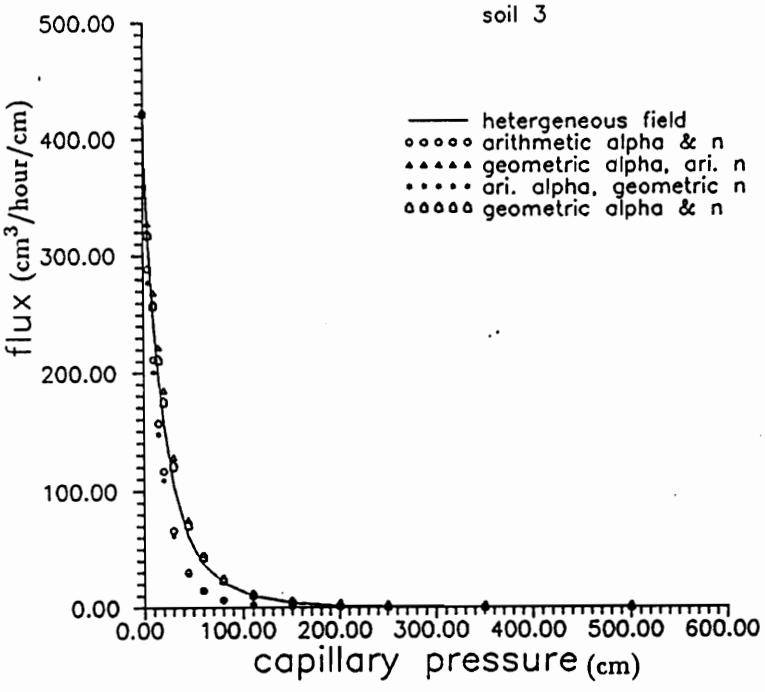


Figure 5.7 Comparison of flux predicted by using arithmetic, geometric mean property and heterogeneous medium for soil No.3

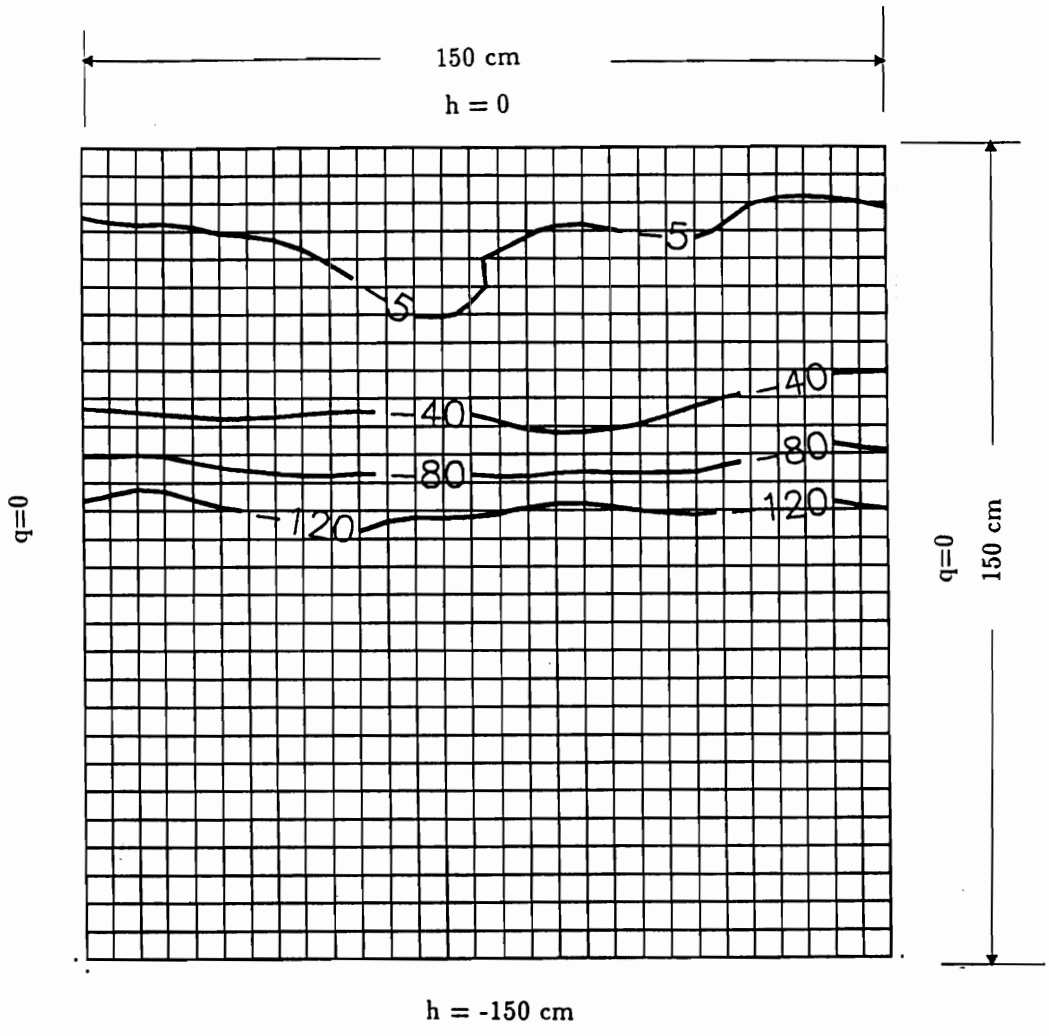


Figure 5.8 Geometry and boundary conditions for transient infiltration simulations and head distribution at time t=1.1 hour for a single realization

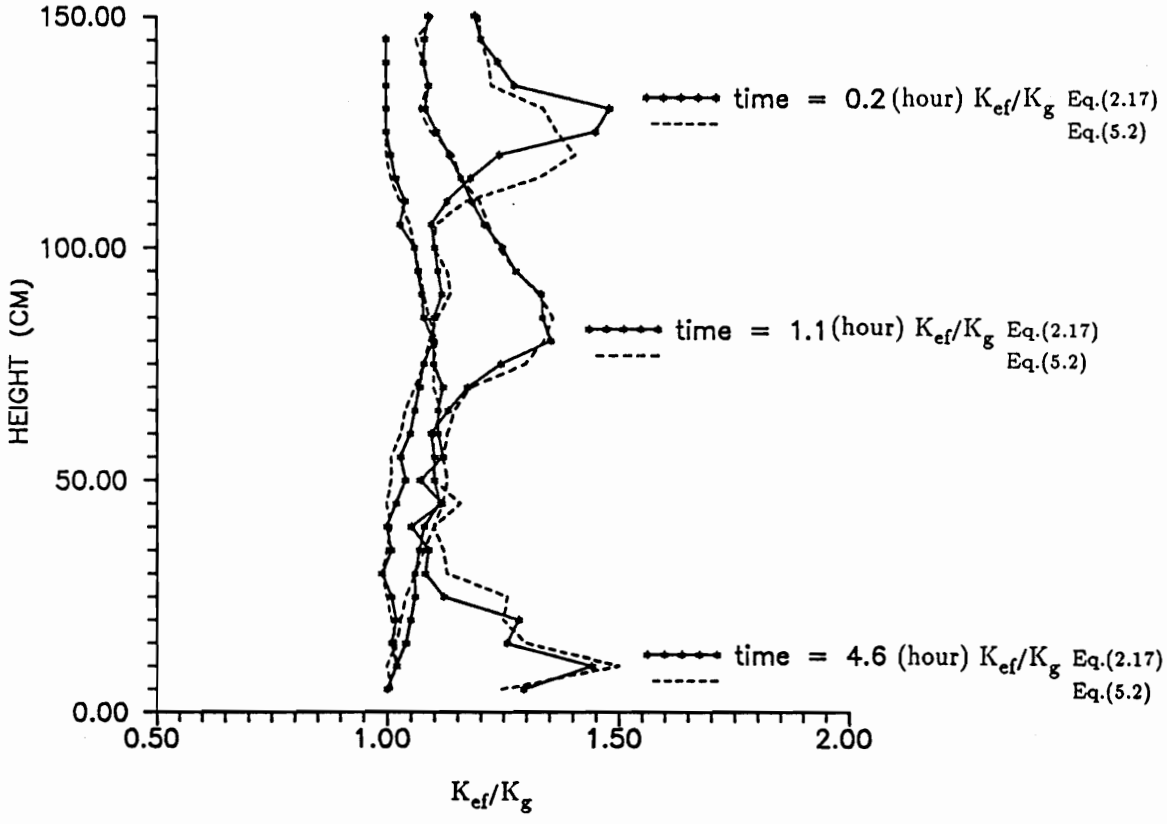


Figure 5.9 Distribution of ratios of effective conductivity over geometric mean of conductivity at different times

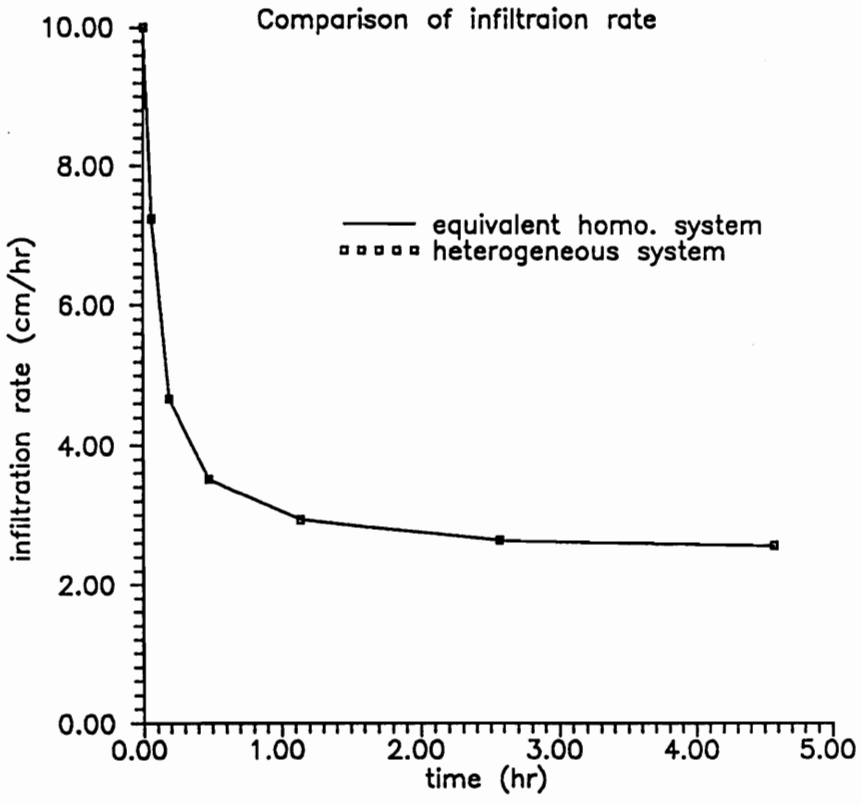


Figure 5.10 Comparison of infiltration between Monte Carlo simulation results and that predicated with effective properties for transient infiltration flow

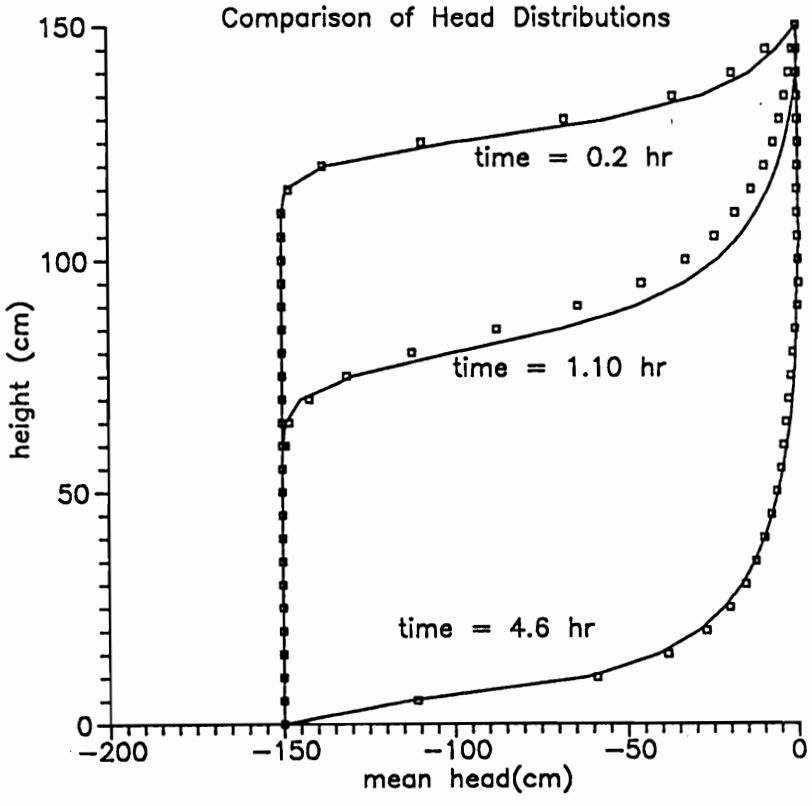


Figure 5.11 Cmparison of head distribution predicted by using effective properties and that of Monte Carlo simulations

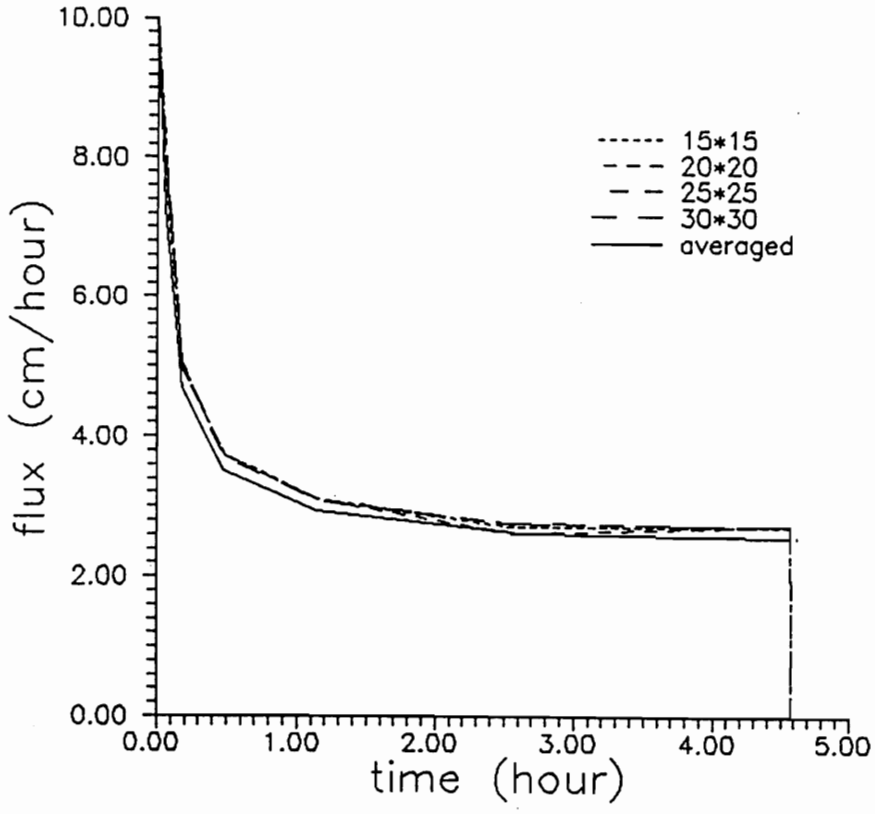


Figure 5.12 Comparisons of fluxes for different mesh systems

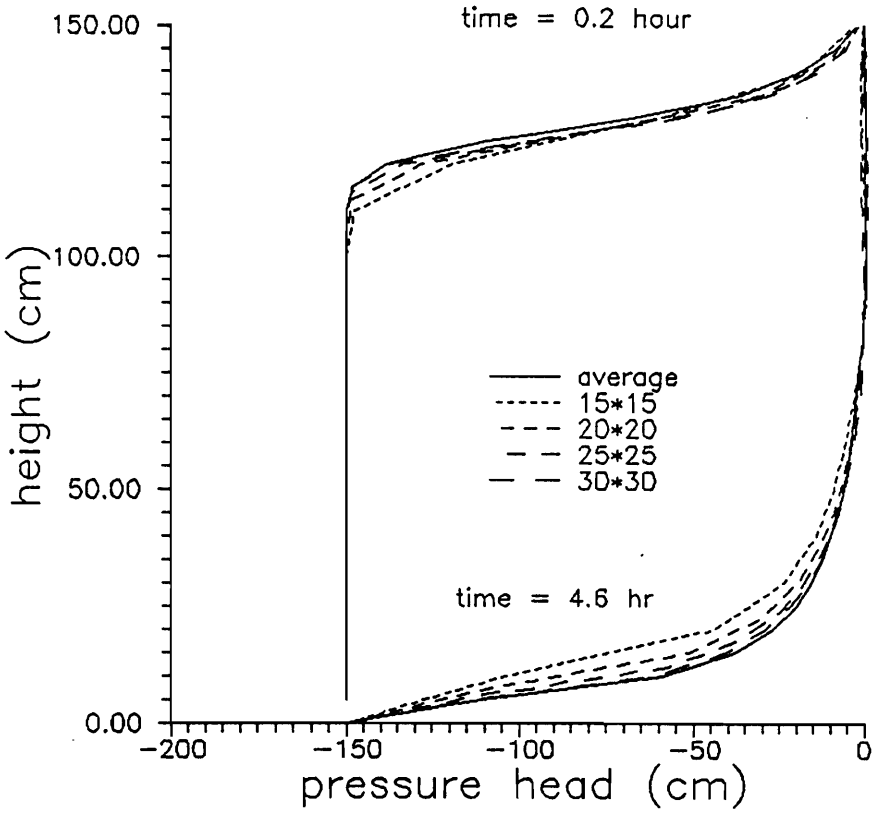


Figure 5.13 Comparisons of head ditributions for different mesh systems during infiltration

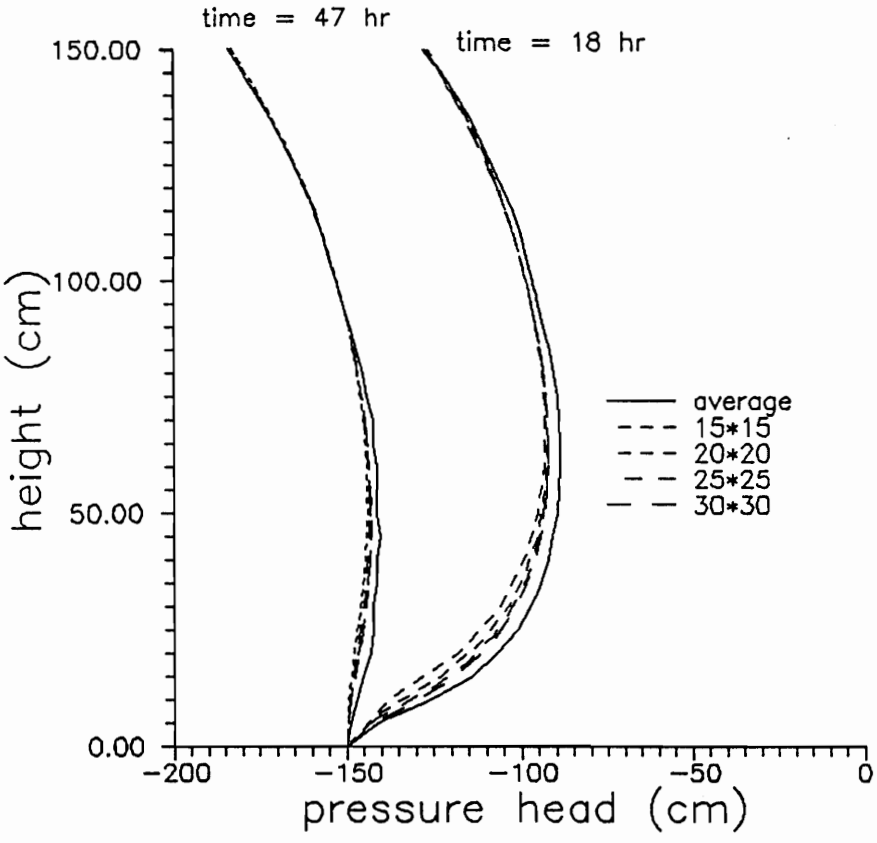


Figure 5.14 Comparisons of head distributions for different mesh systems during redistribution

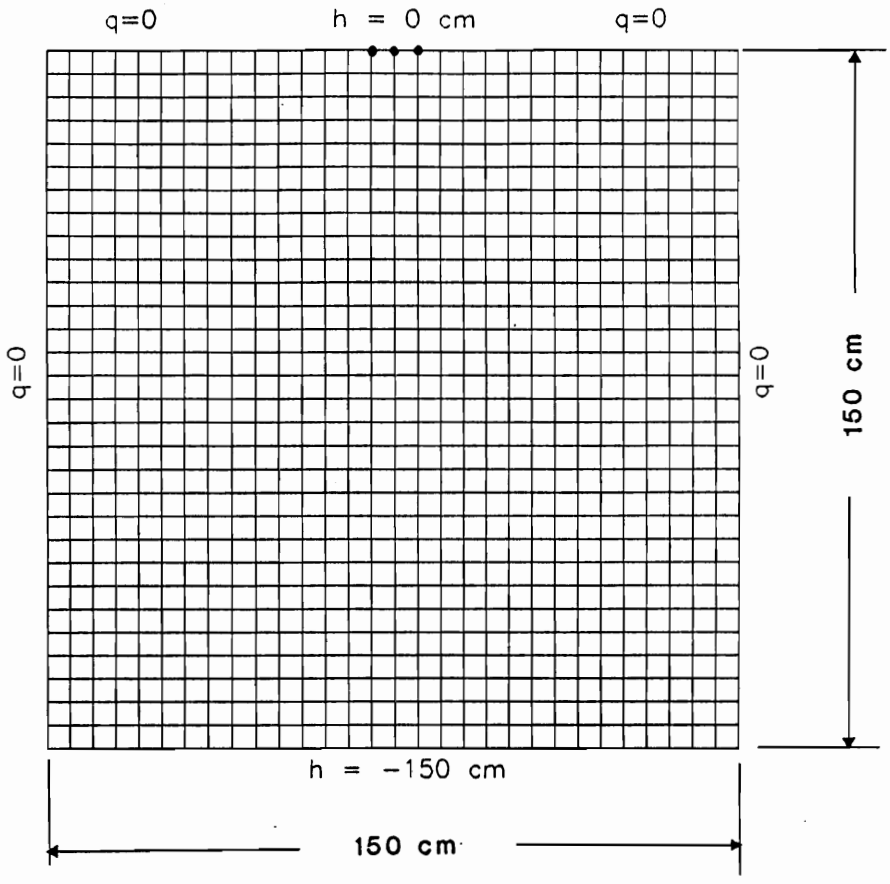


Figure 5.15 Domain geometry and boundary condition for 2-D point source infiltration flow simulations

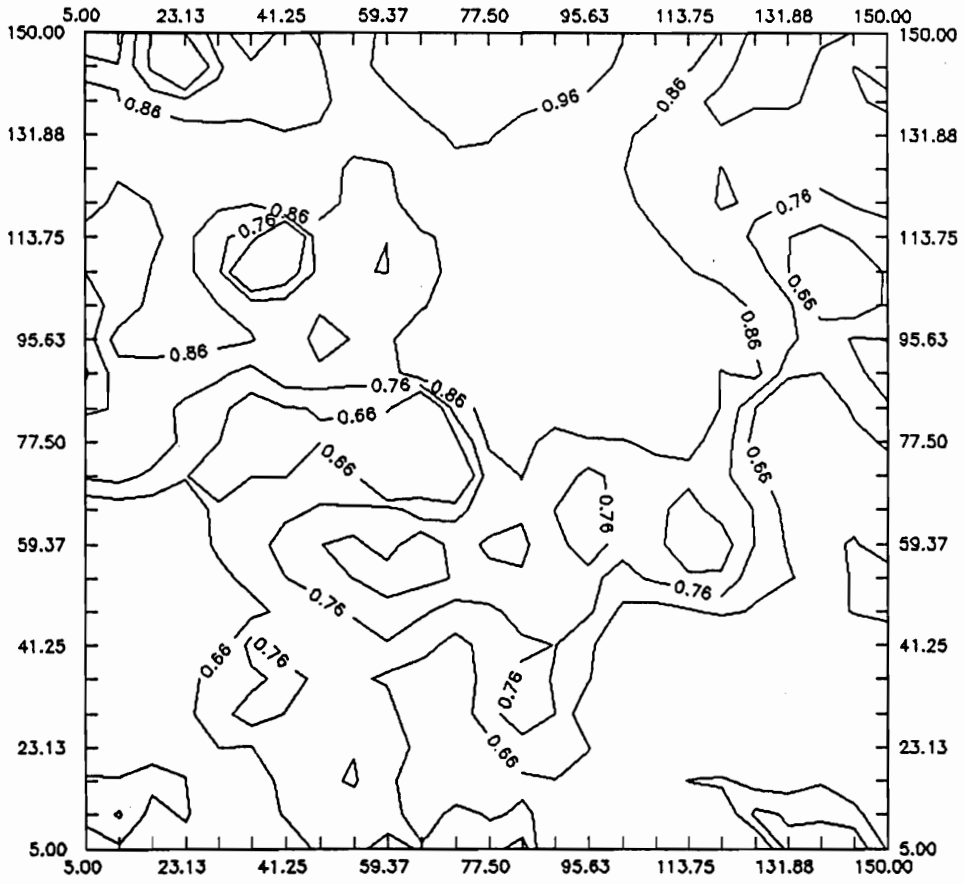


Figure 5.16 Saturation distribution for a single realization at time $t = 3.4$ *hour*

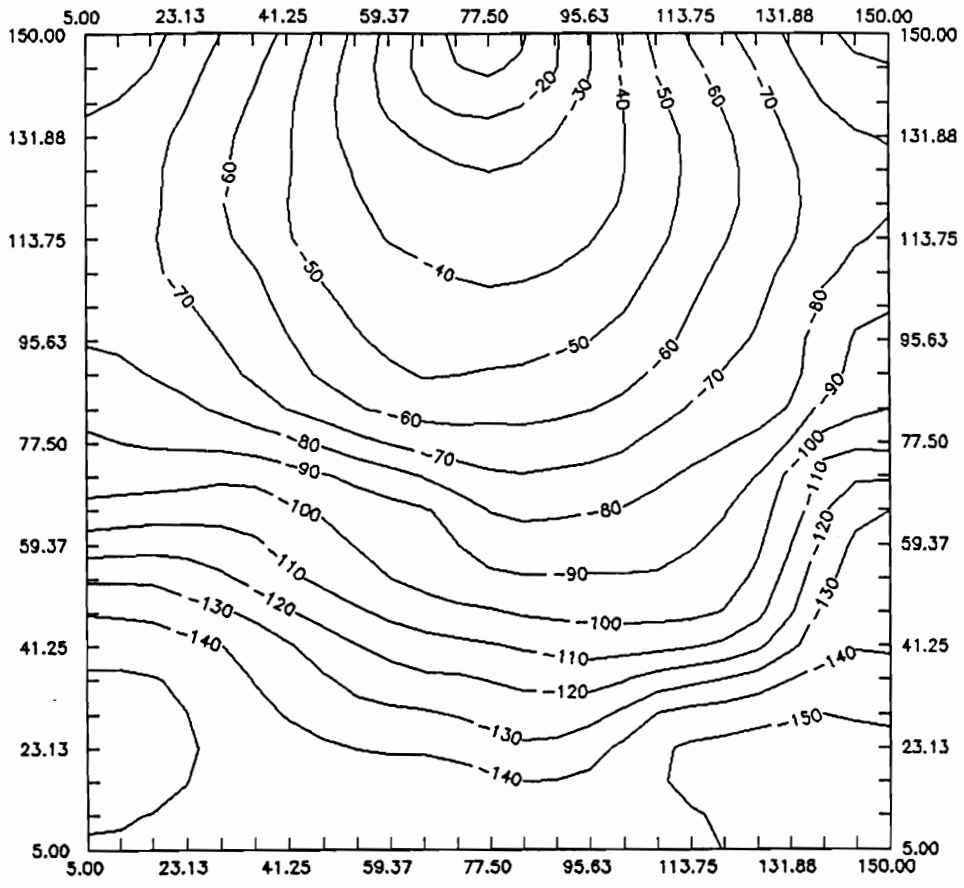


Figure 5.17 Pressure head distribution for a single realizatons at time $t = 3.4$ *hour*

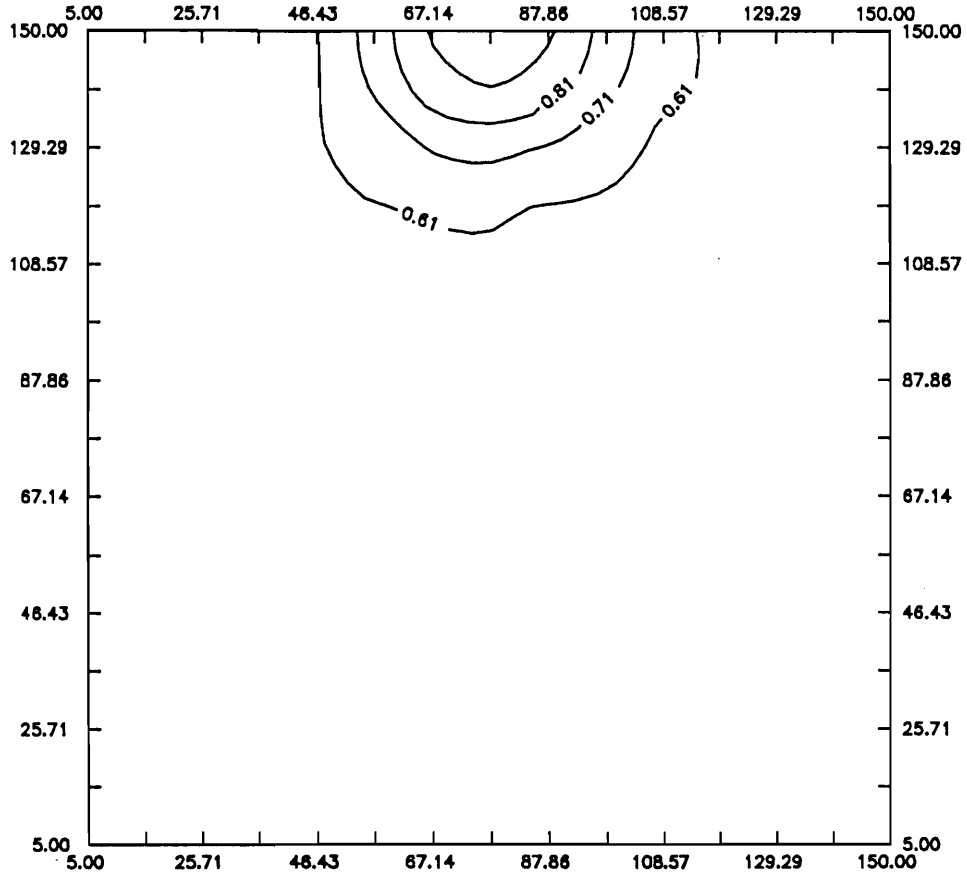


Figure 5.18 Contours of saturatons at time $t = t_4$

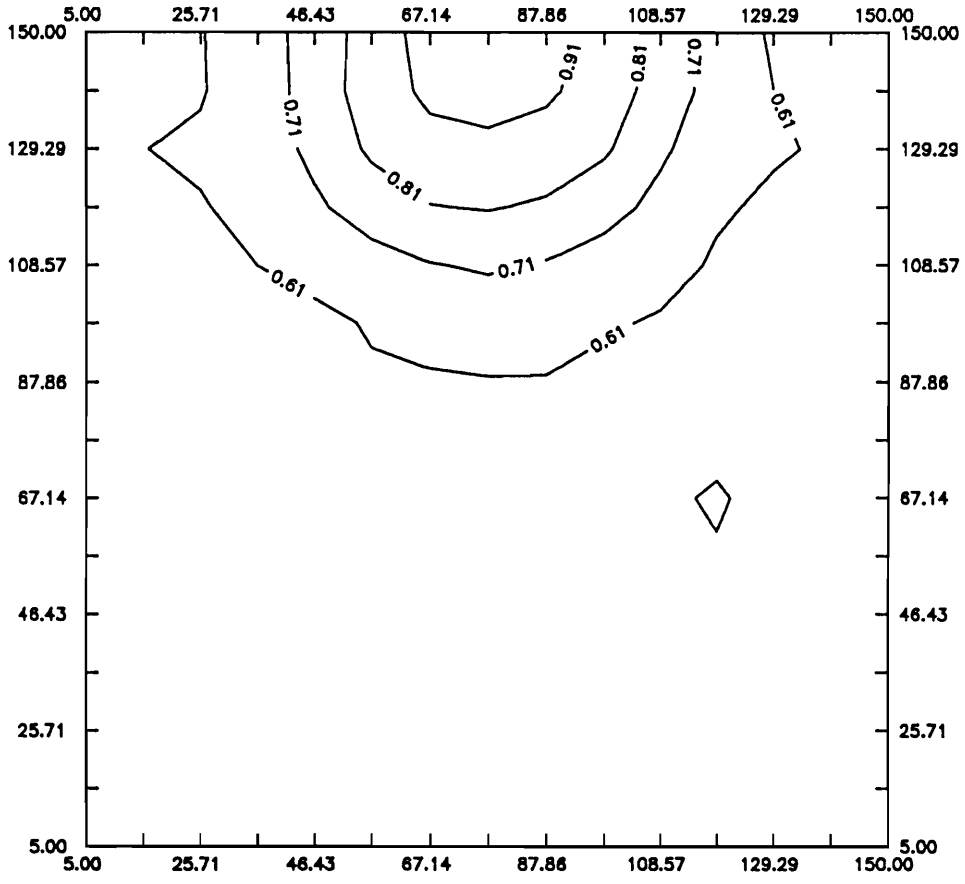


Figure 5.19 Contours of saturatons at time $t = t_5$

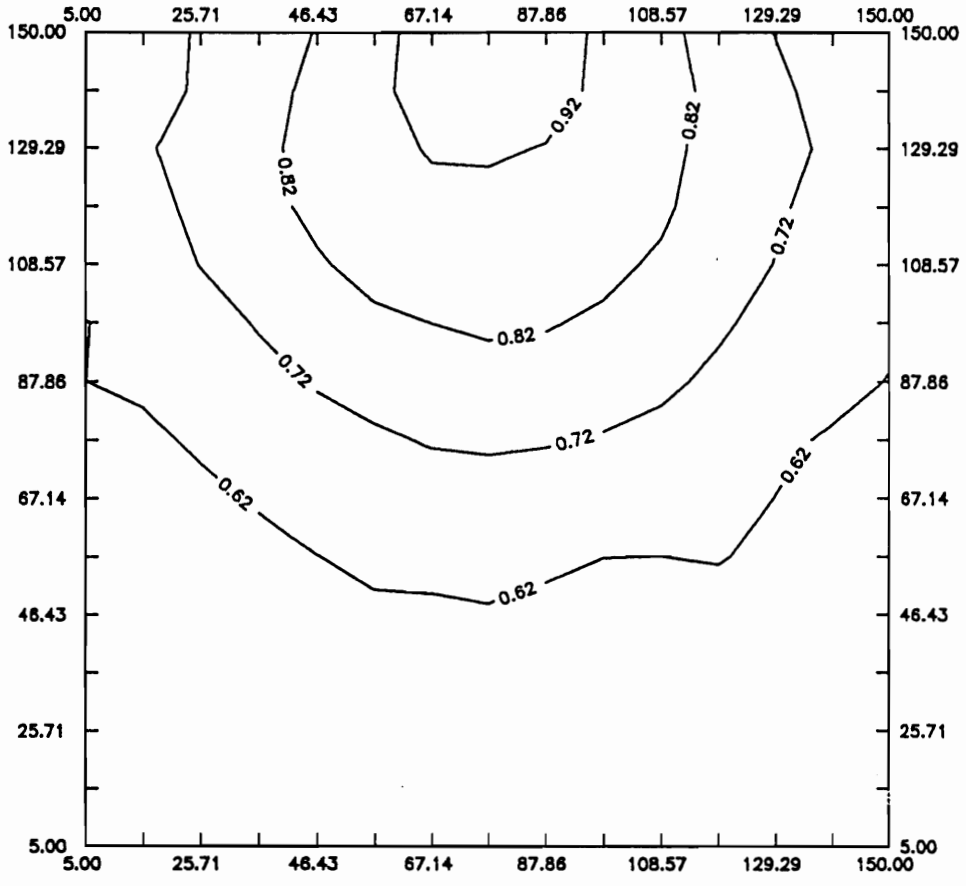


Figure 5.20 Contours of saturation at time $t = t_6$

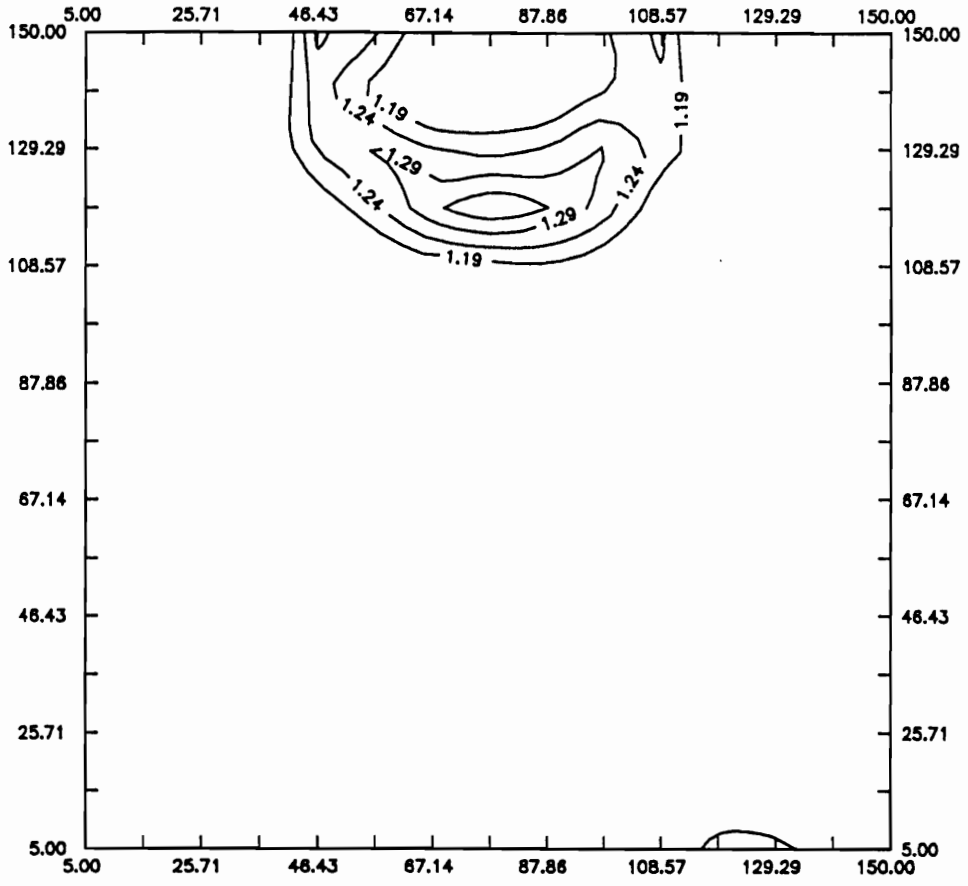


Figure 5.21 Distributions of ratios of effective conductivity in Z directon over geometric mean of conductivity at time $t = t_4$

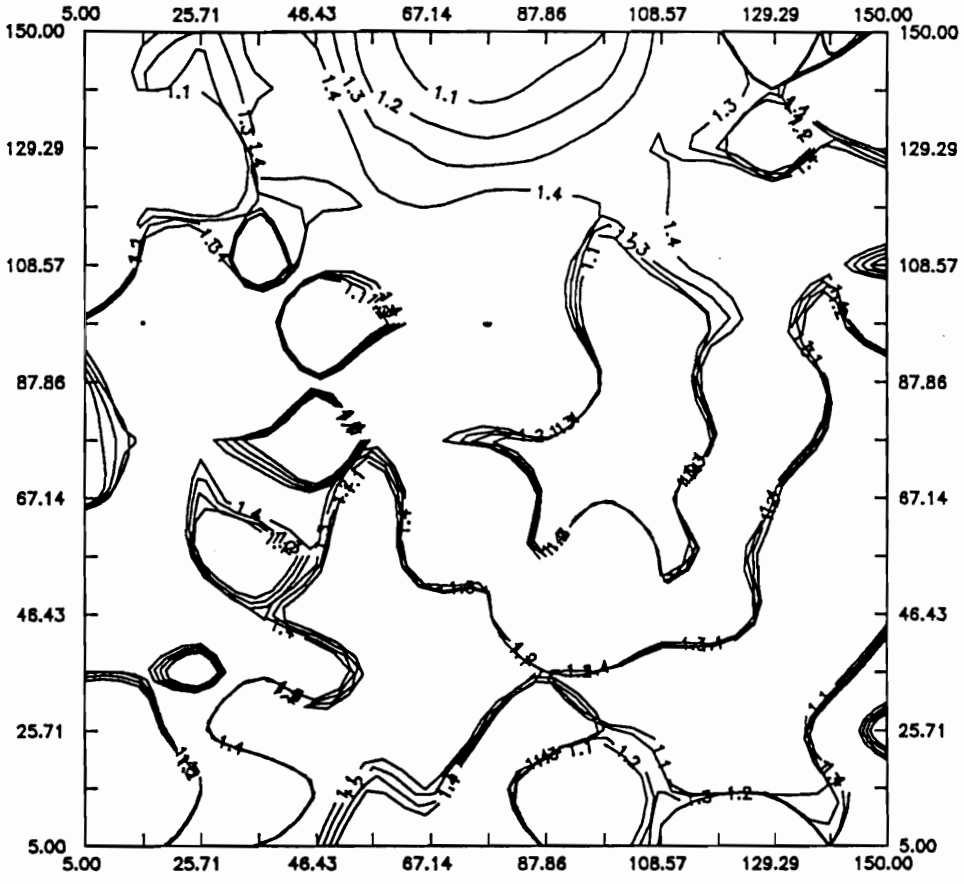


Figure 5.22 Distributions of ratios of effective conductivity in X direction over geometric mean of conductivity at time $t = t_4$

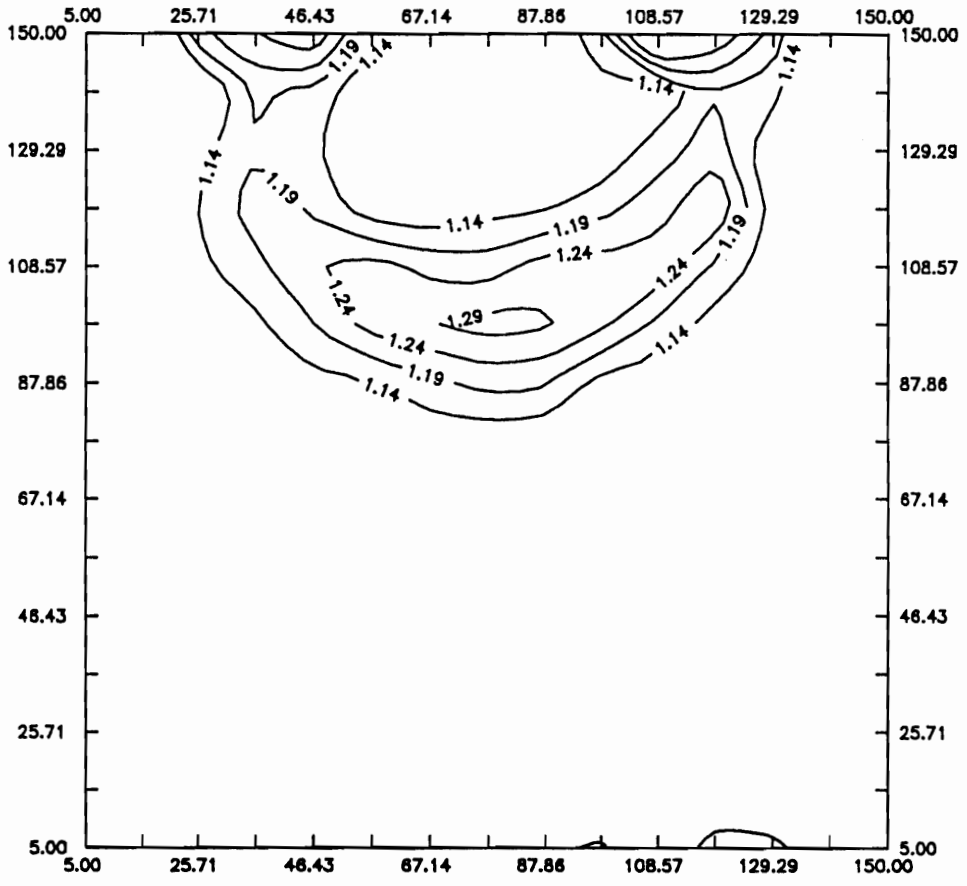


Figure 5.23 Distributions of ratios of effective conductivity in Z direction over geometric mean of conductivity at time $t = t_5$

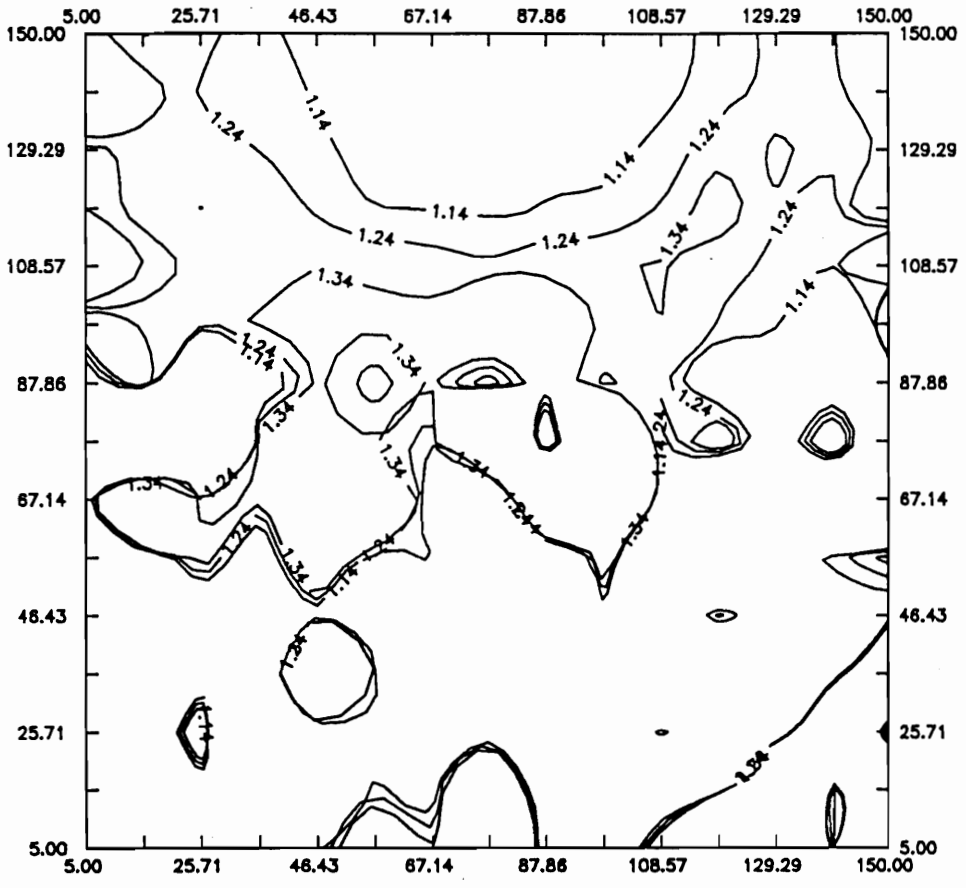


Figure 5.24 Distributions of ratios of effective conductivity in X directon over geometric mean of conductivity at time $t = t_5$

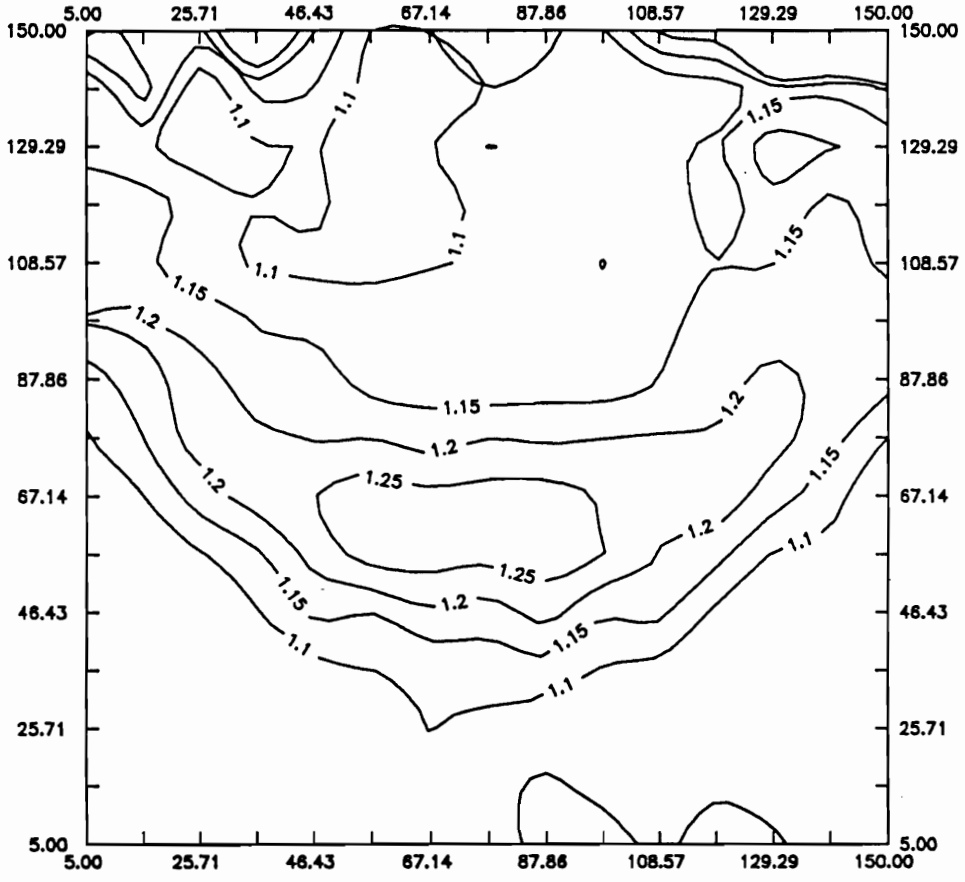


Figure 5.25 Distributions of ratios of effective conductivity in Z direction over geometric mean of conductivity at time $t = t_6$

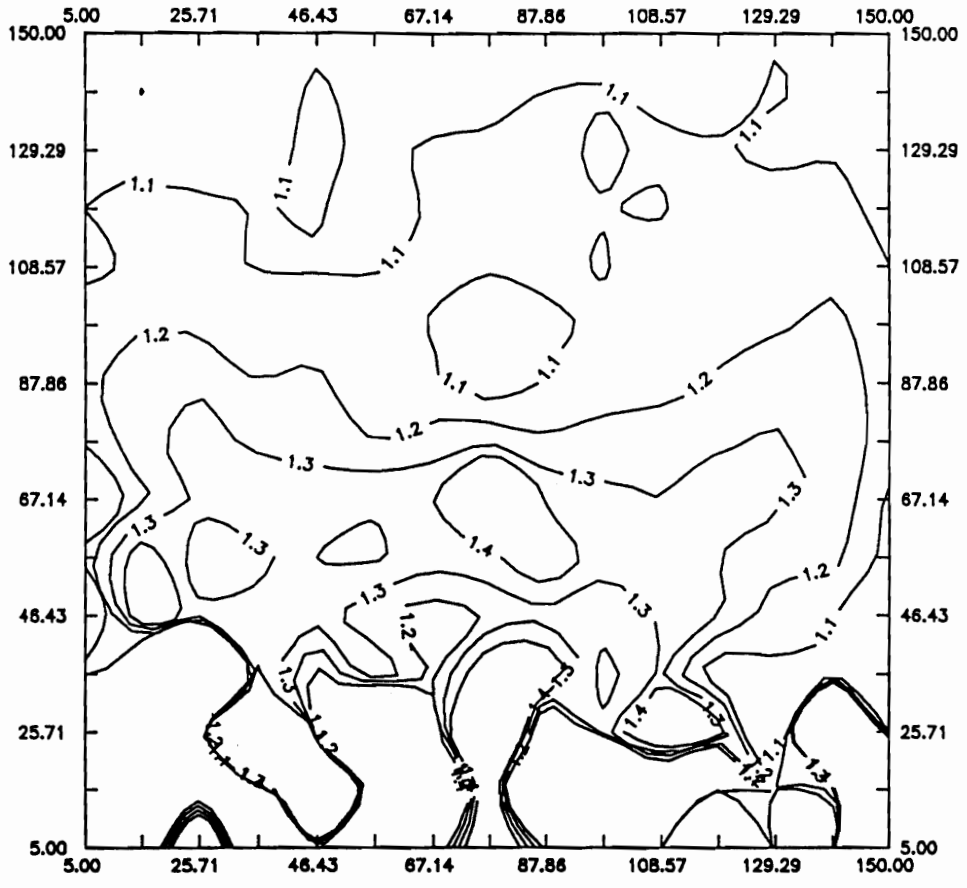


Figure 5.26 Distributions of ratios of effective conductivity in X direction over geometric mean of conductivity at time $t = t_6$

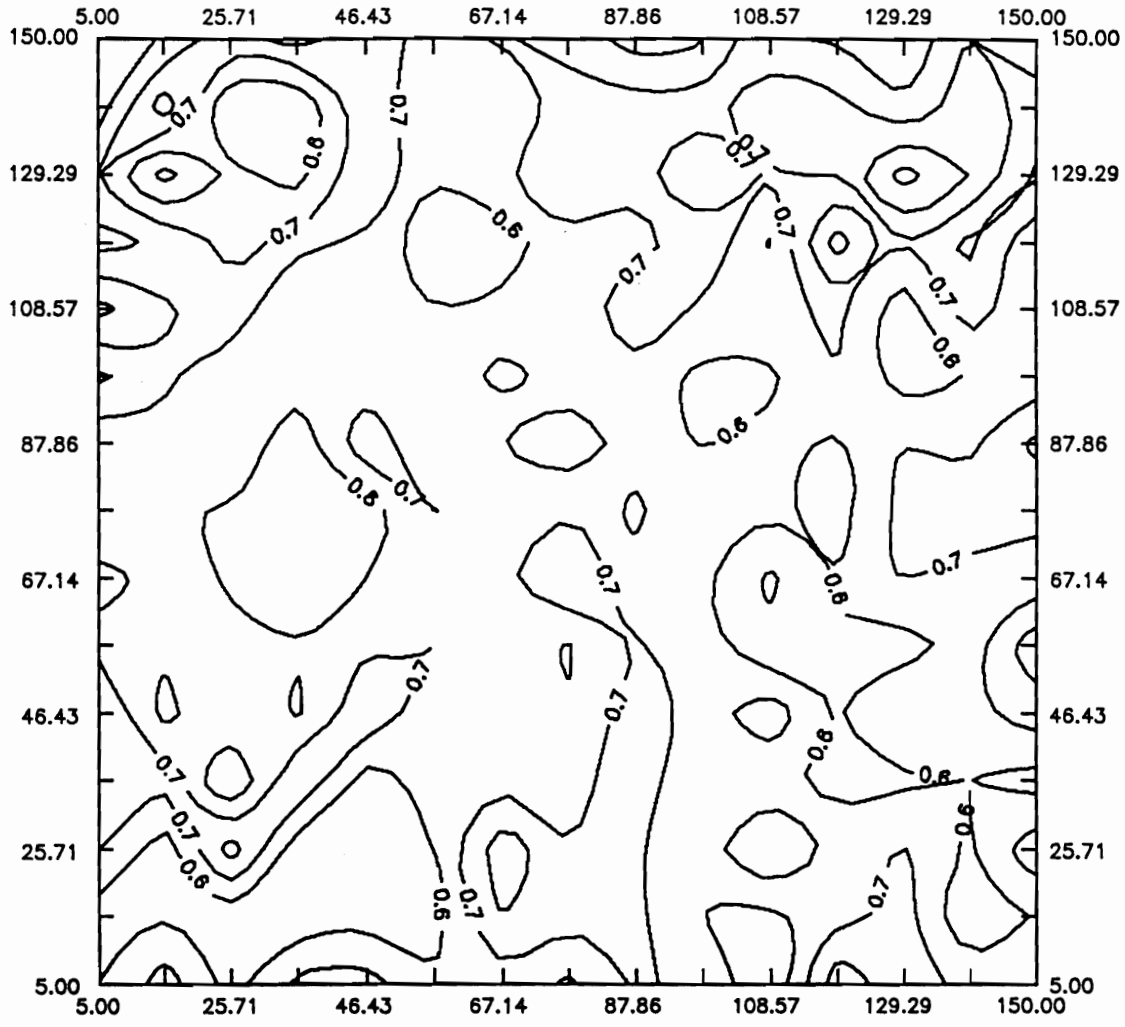


Figure 5.27 Distributions of variance of log unsaturated conductivity

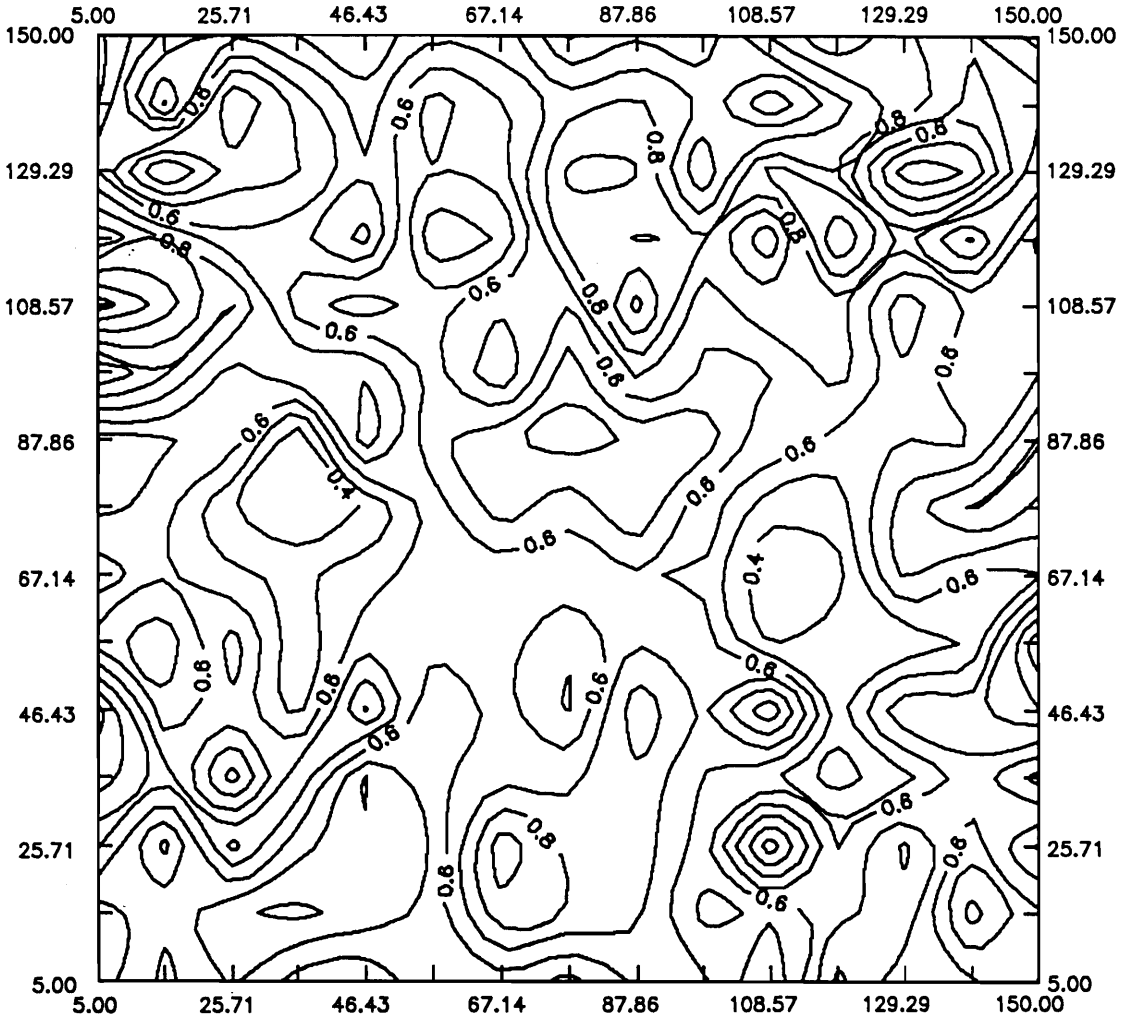


Figure 5.28 Distributions of variance of log saturated conductivity

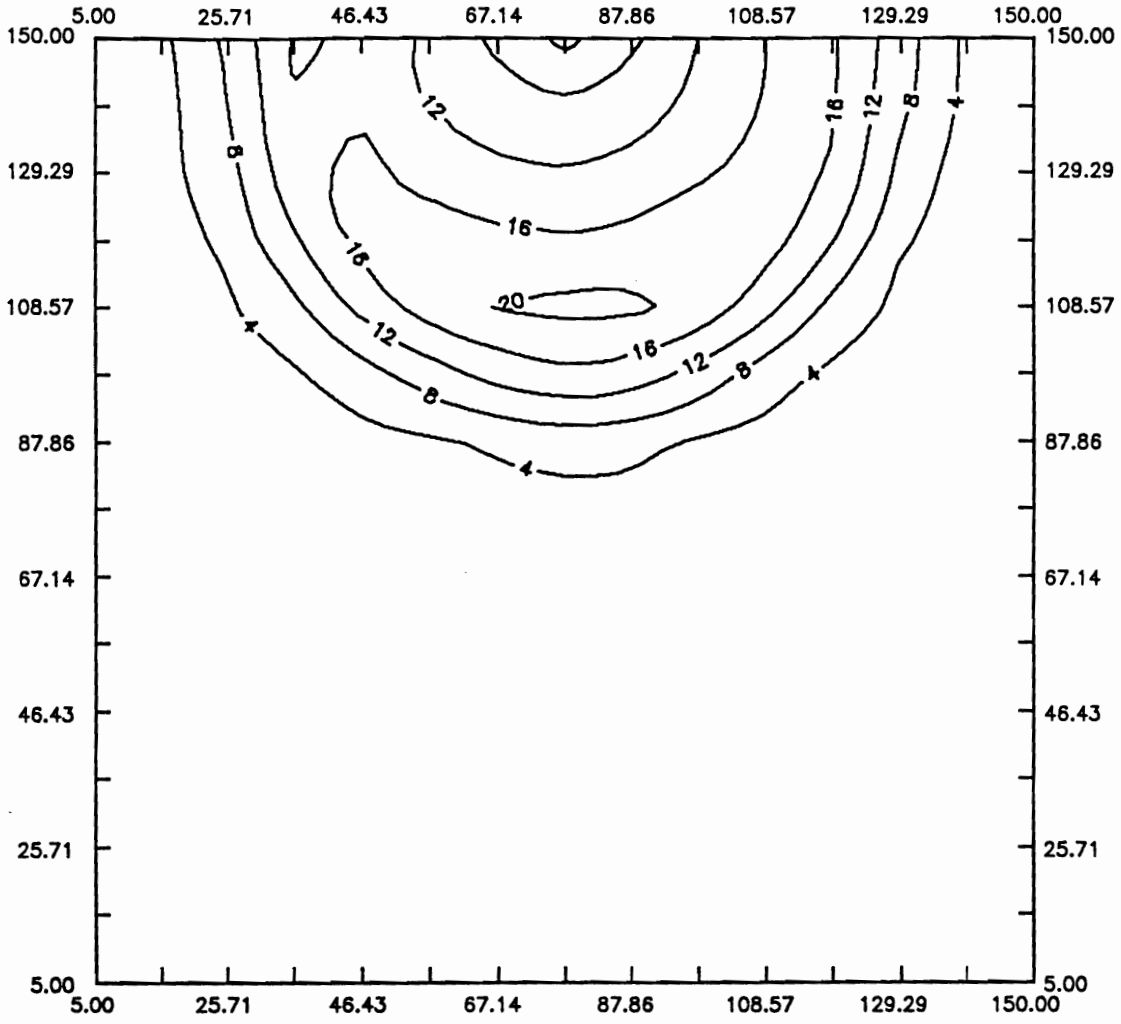


Figure 5.29 Contours of variance of pressure head at time $t = t_5$

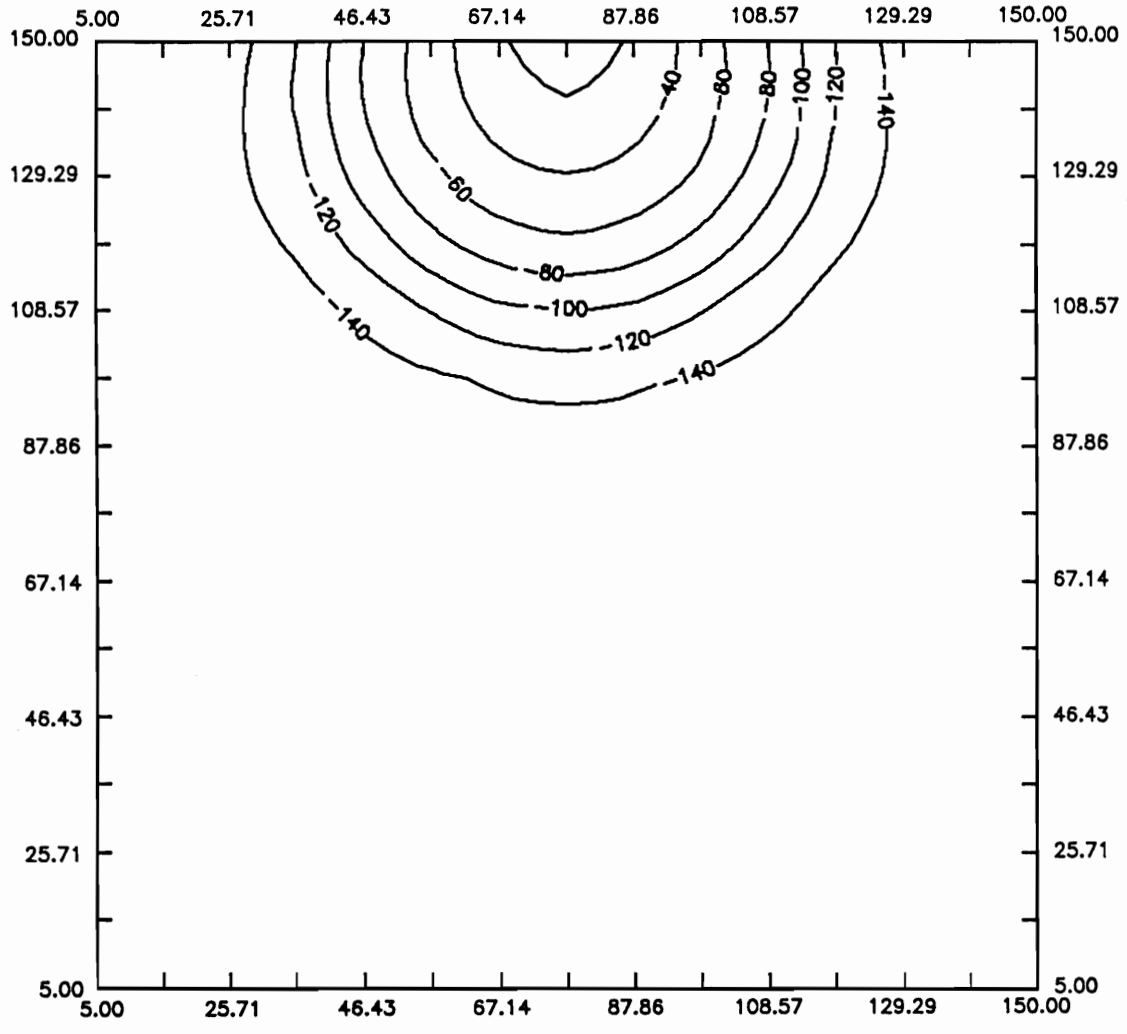


Figure 5.30 Head distributions predicted by mean model at time $t = t_5$

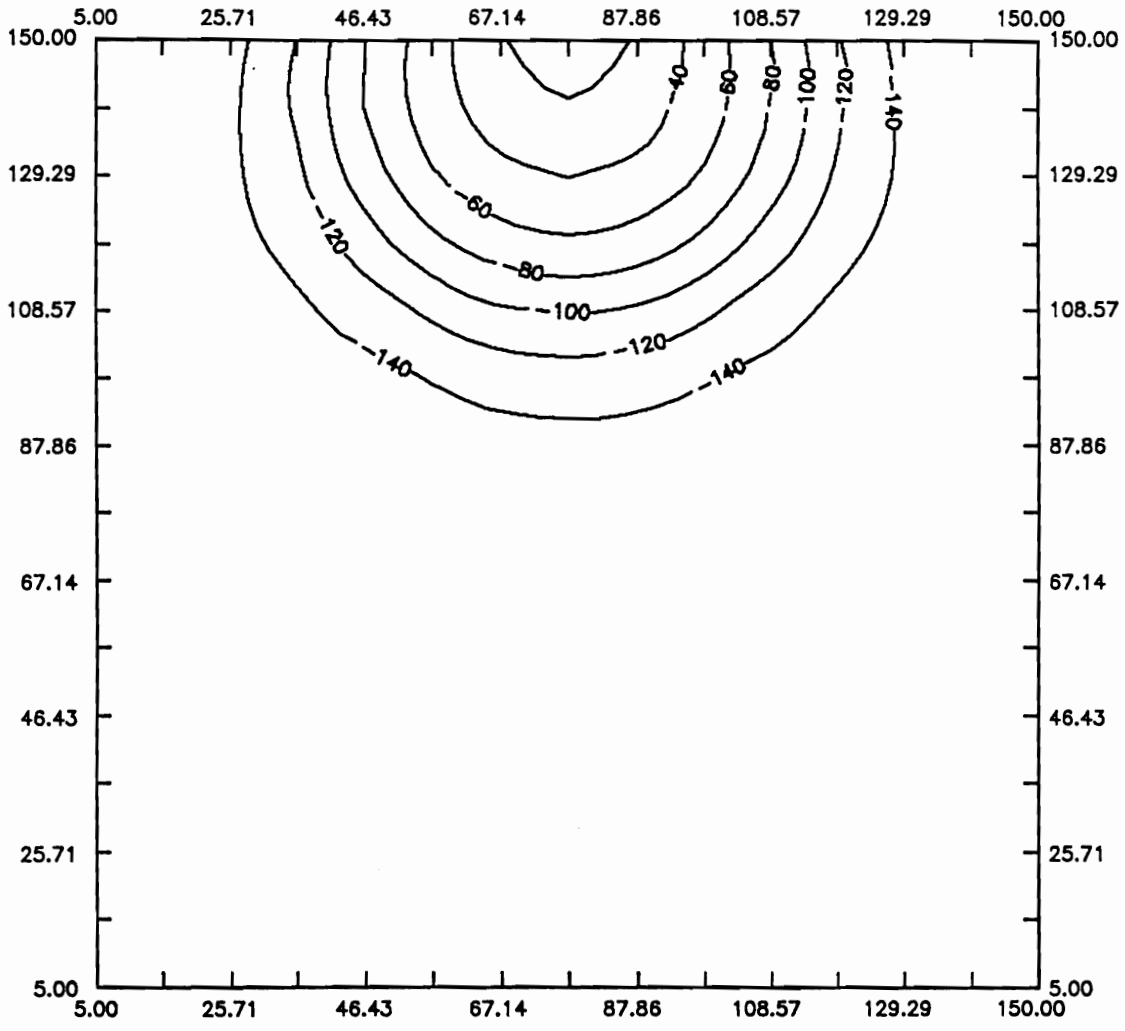


Figure 5.31 Head distributions of Monte Carlo simulations at time $t = t_5$

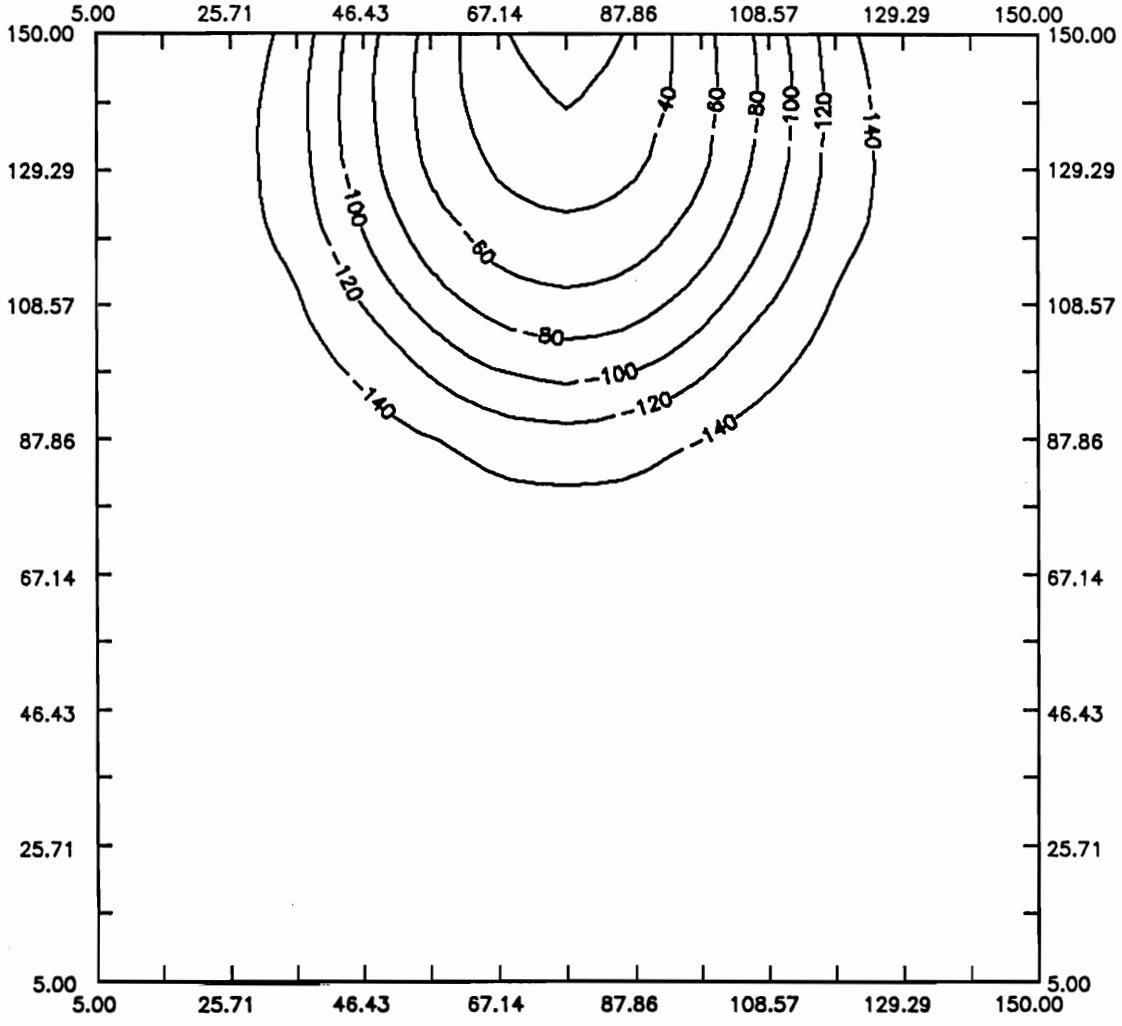


Figure 5.32 Head distributions predicted by classical model at time $t = t_5$

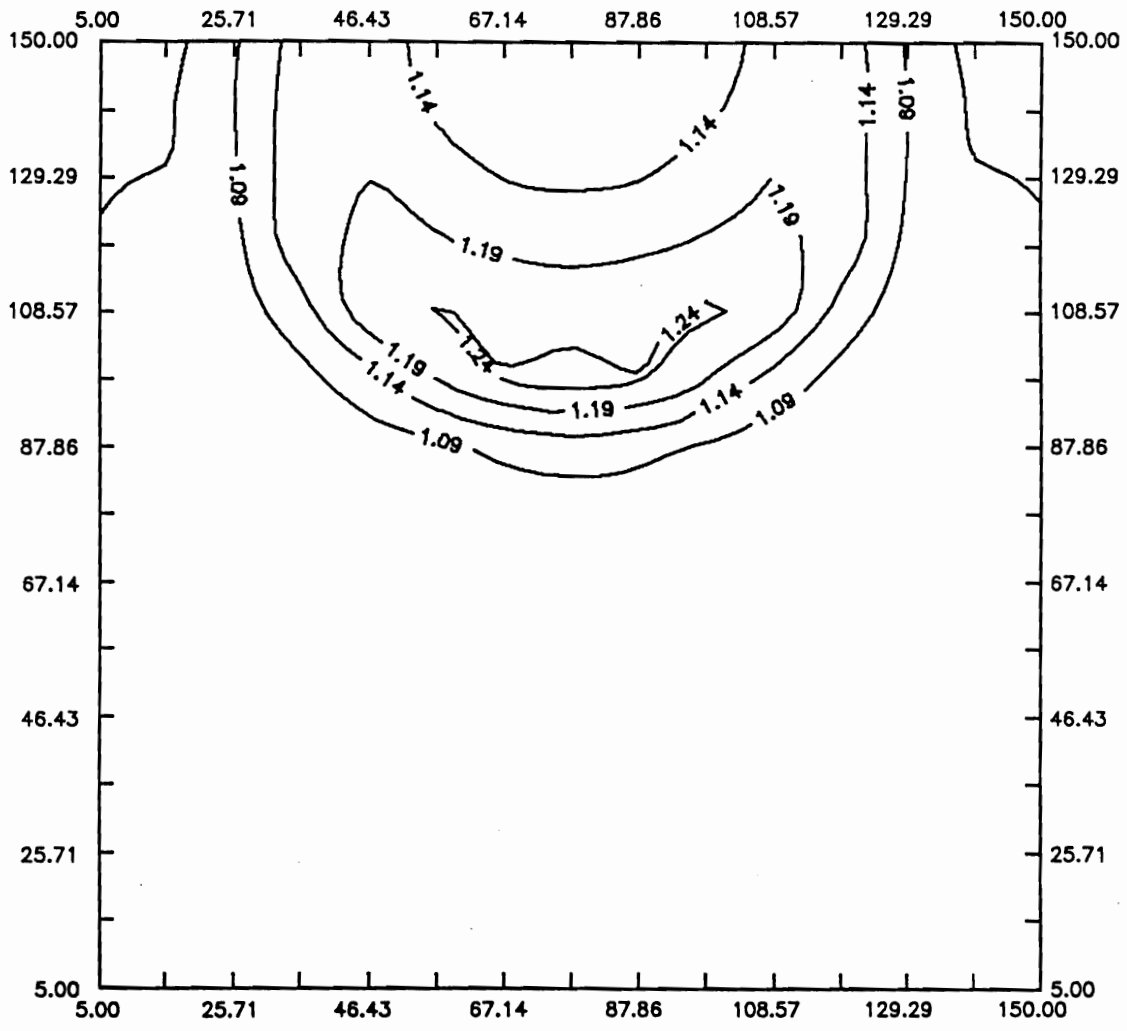


Figure 5.33 $K_{ef}/K_g$ calculated by the mean model at time $t = t_5$

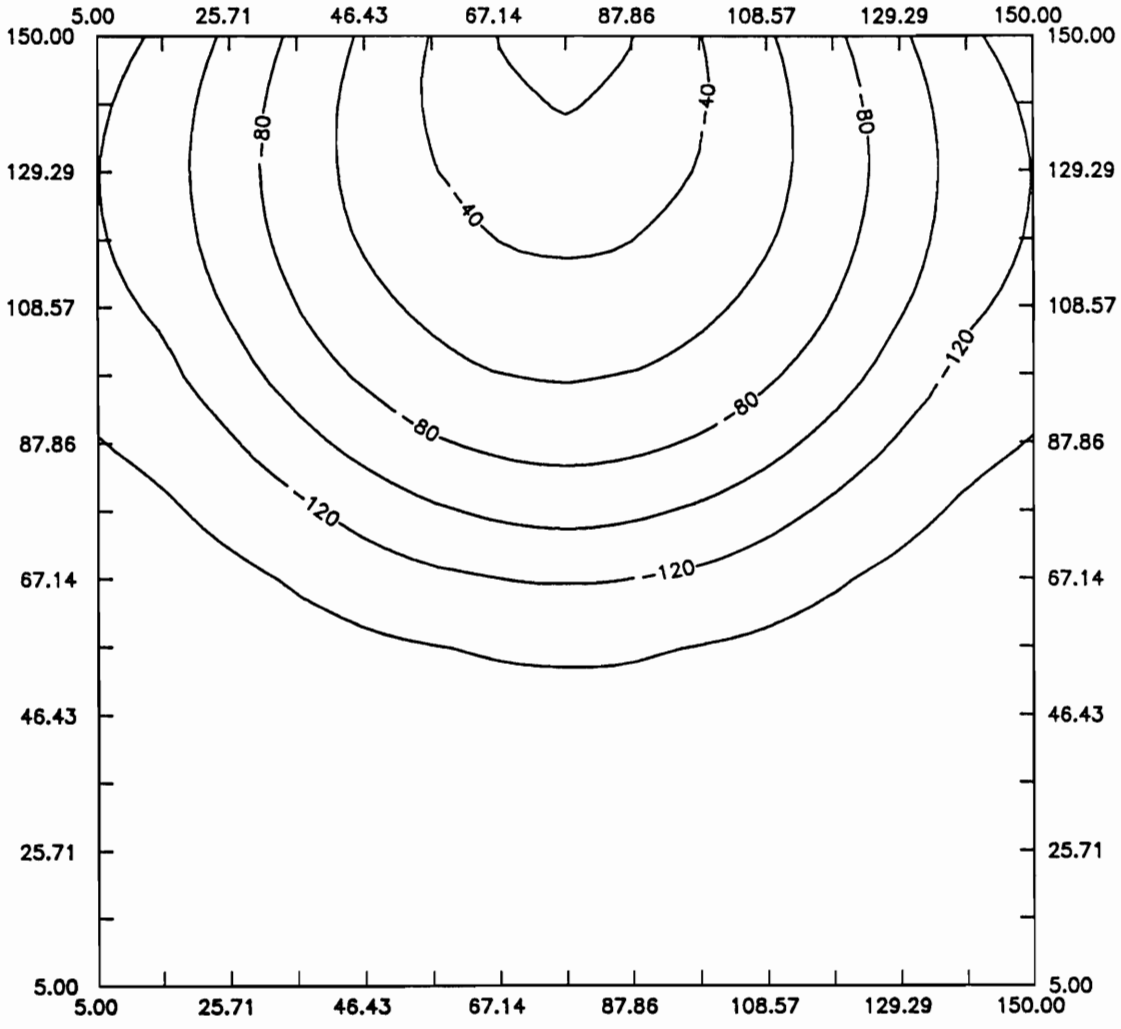


Figure 5.34 Head distributions predicted by the mean model at time $t = t_6$

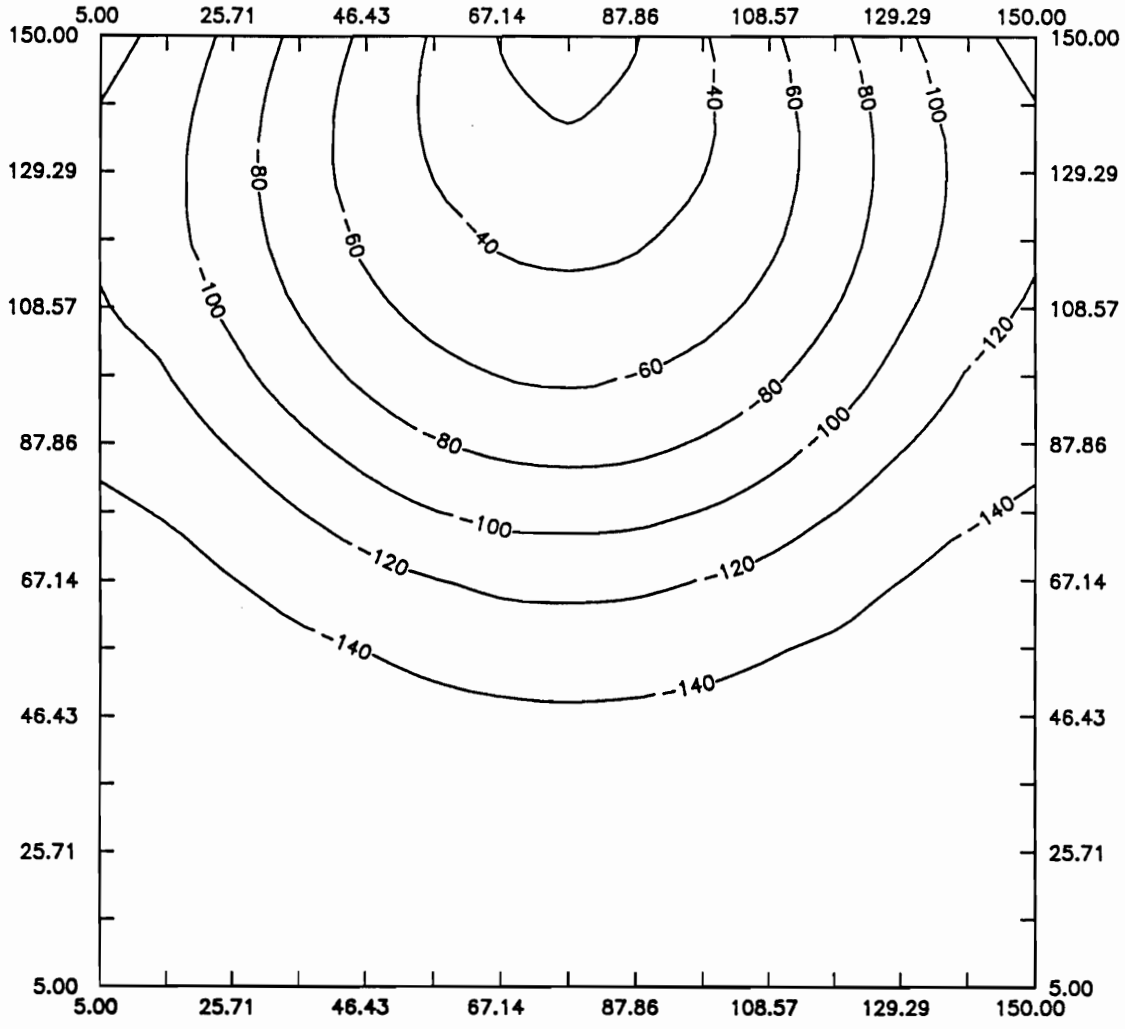


Figure 5.35 Head distributions of Monte Carlo simulations at time $t = t_6$

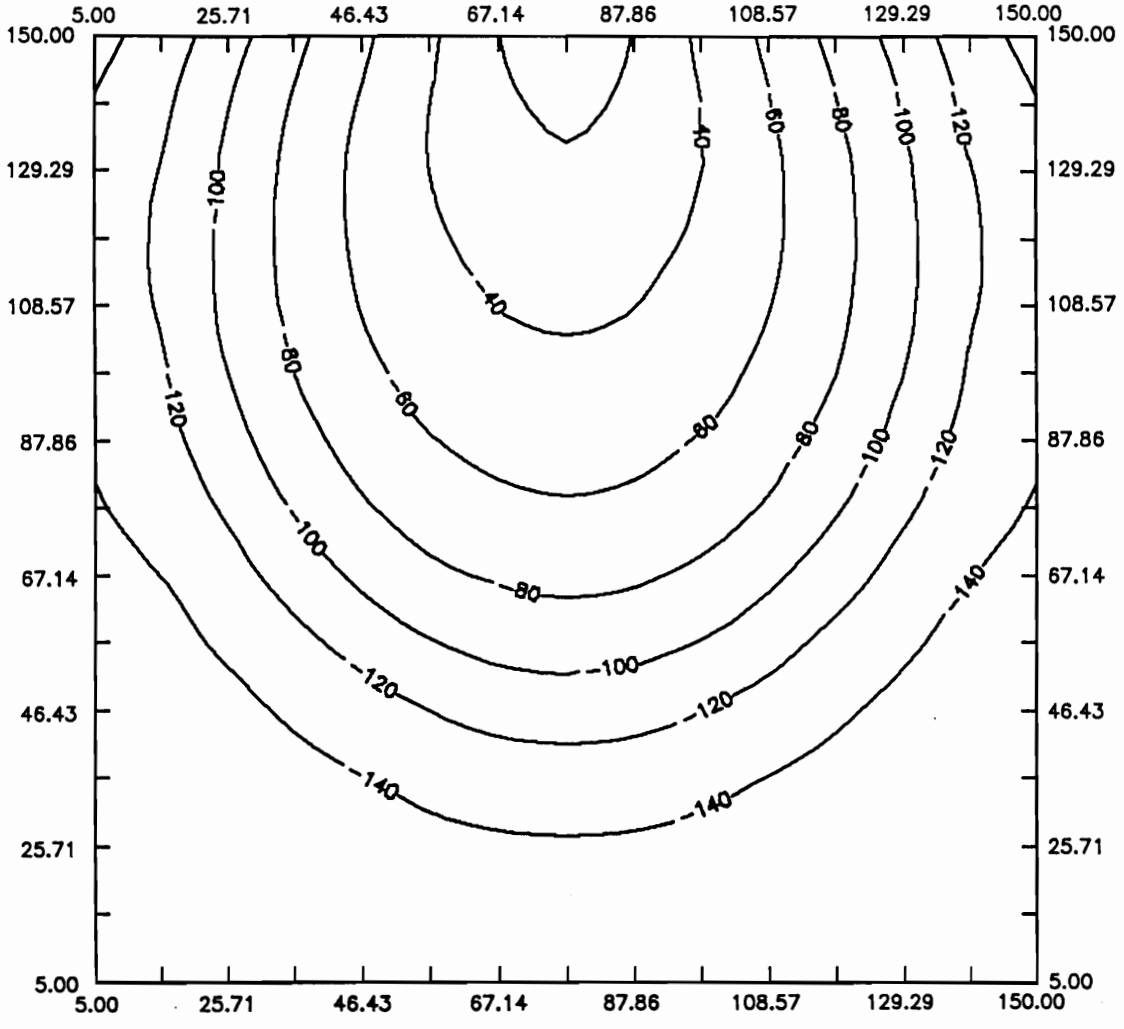


Figure 5.36 Head distributions predicted by classical model at time $t = t_6$

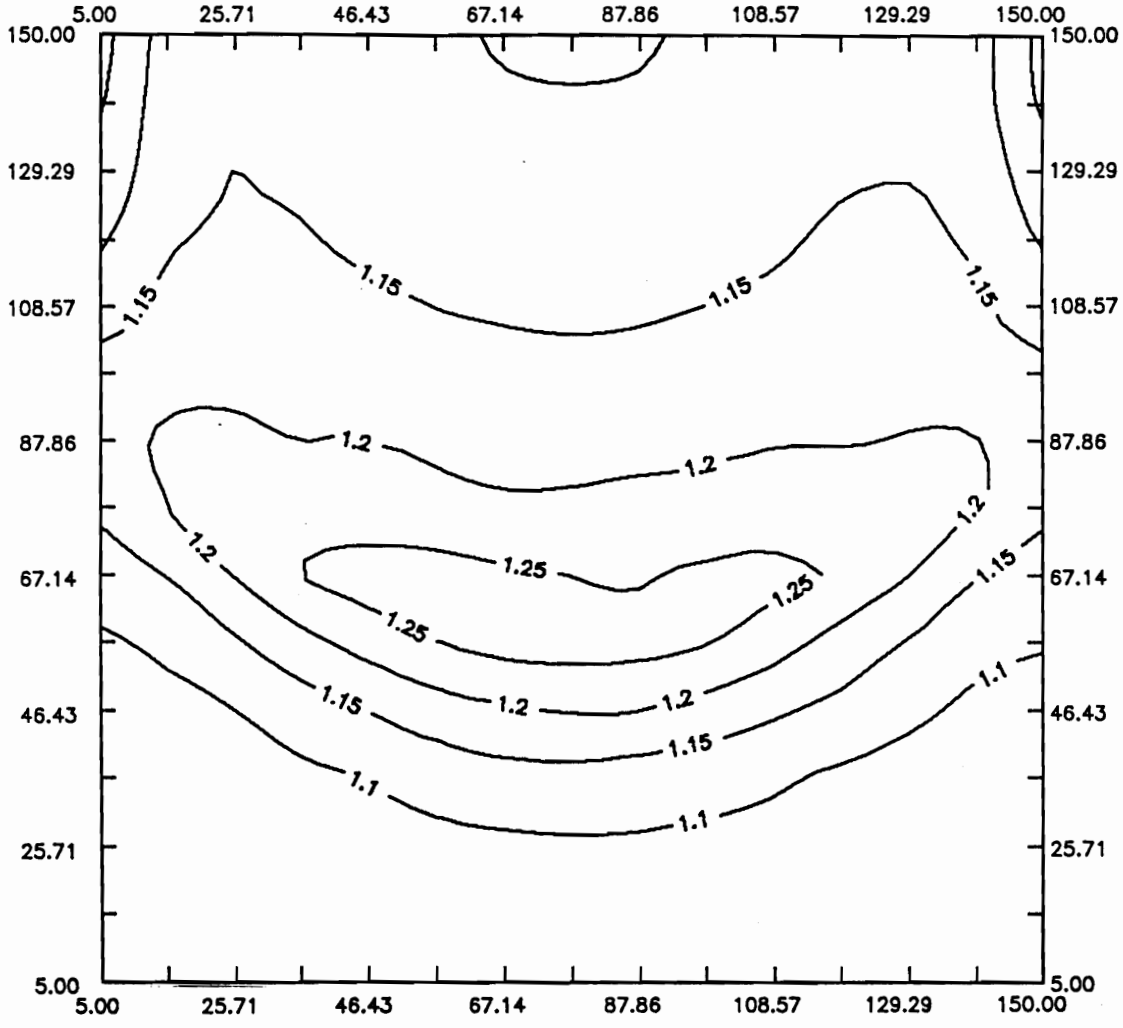


Figure 5.37 $K_{ef}/K_g$ calculated by the mean model at time $t = t_6$

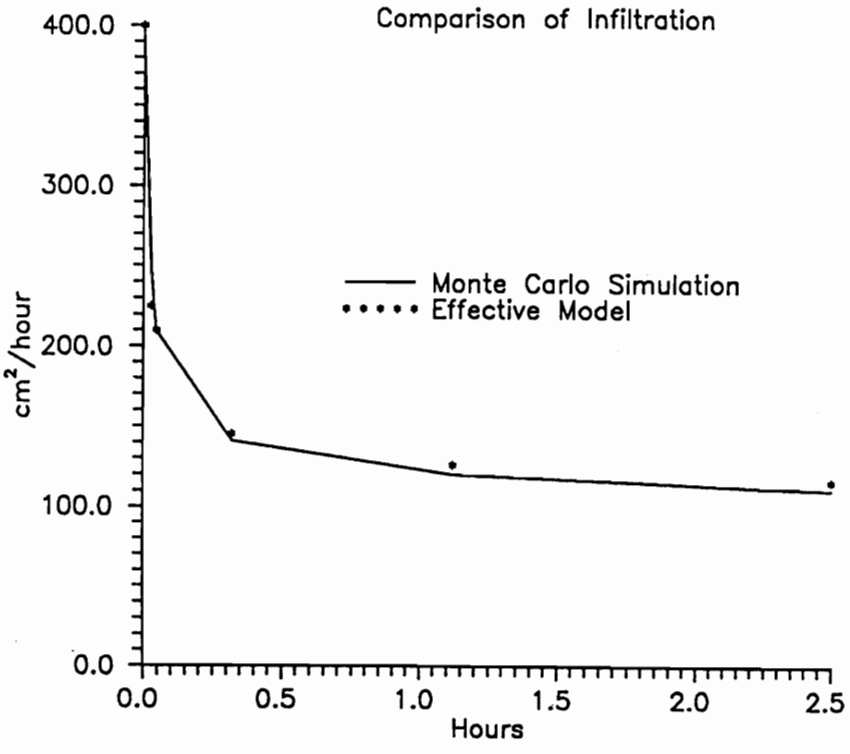


Figure 5.38 Comparison of infiltration of Monte Carlo simulations with that predicted by mean model

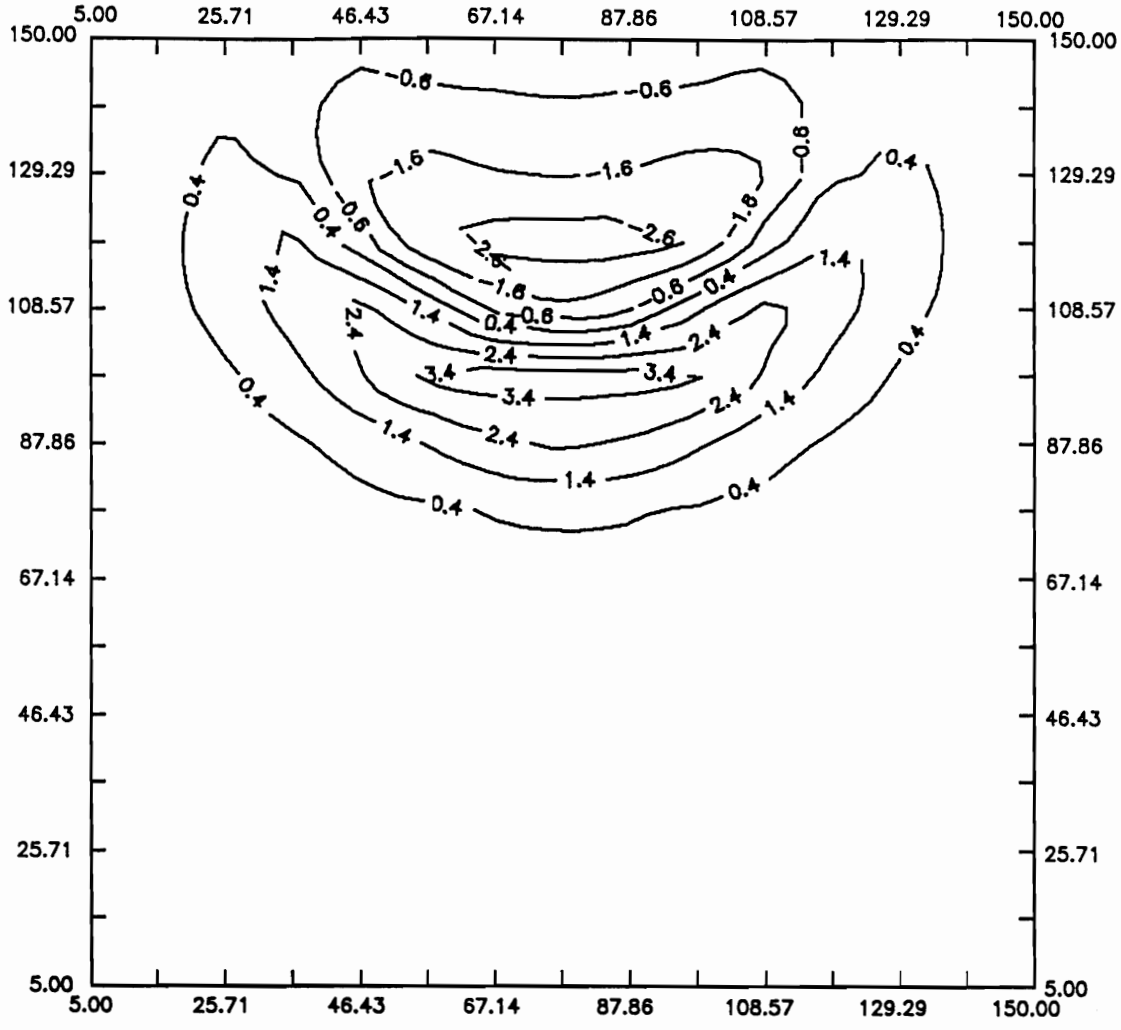


Figure 5.39 Contours of time derivative of head at time $t = t_5$ given by Monte Carlo simulations

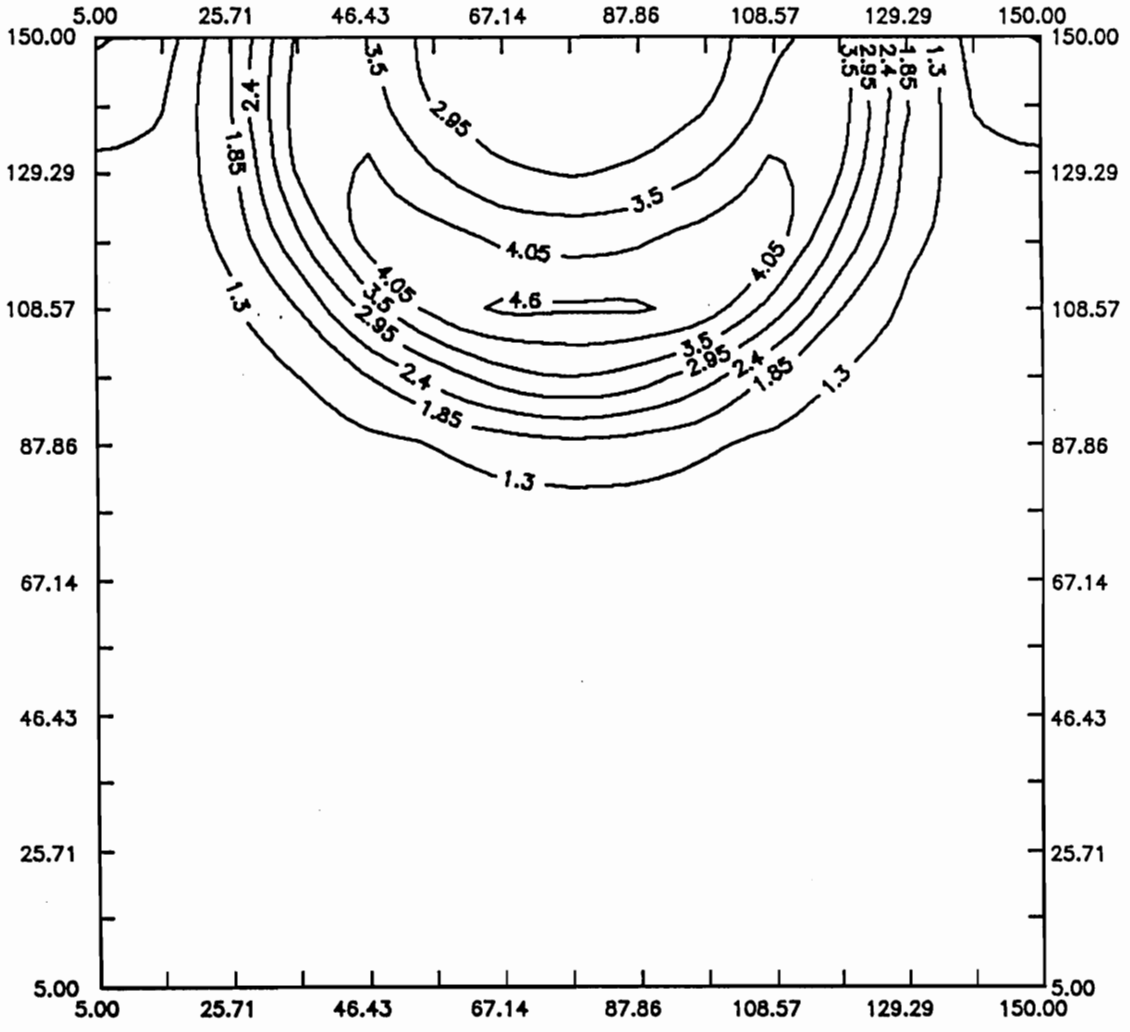


Figure 5.40 Contours of hydraulic gradient at time $t = t_5$ given by Monte Carlo simulations

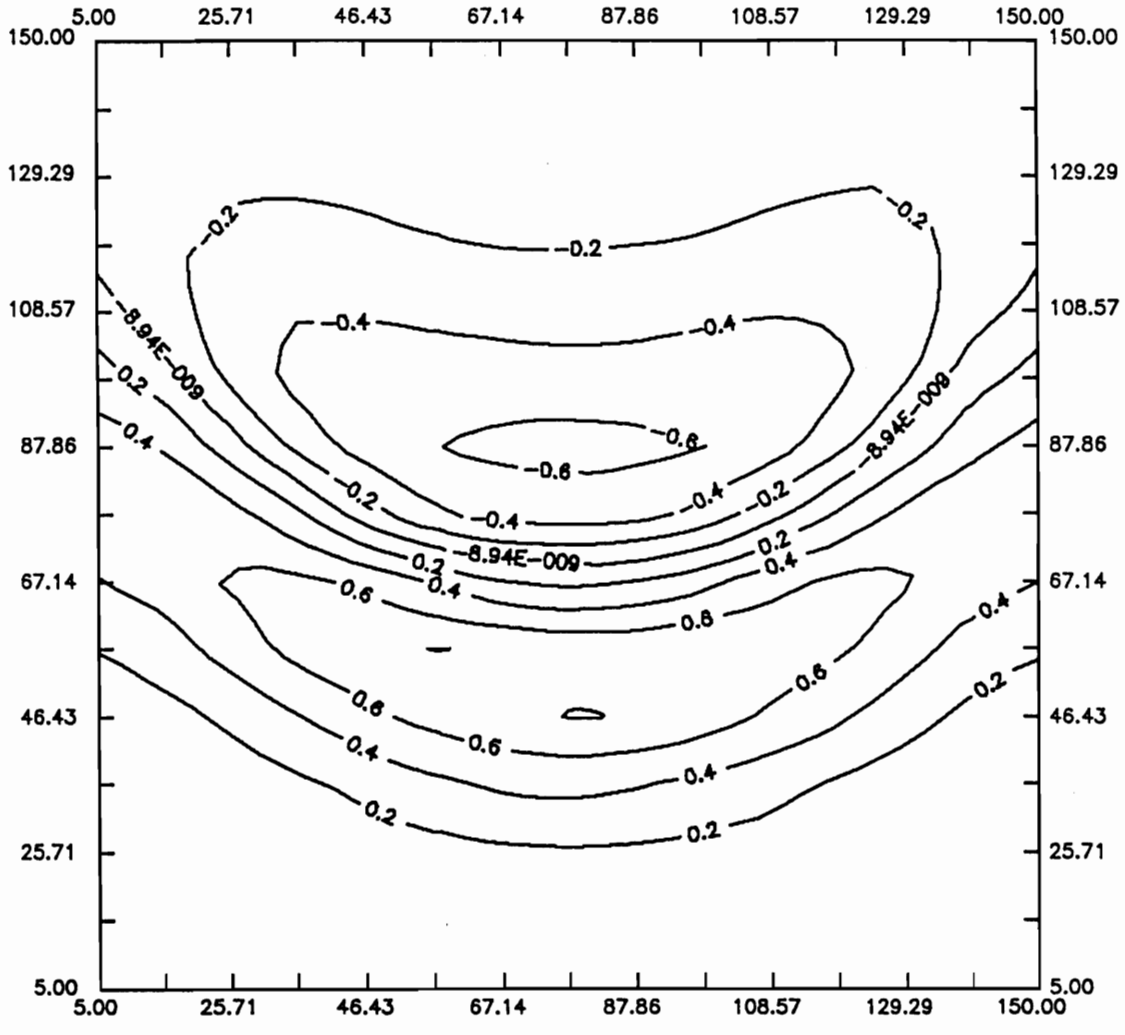


Figure 5.41 Contours of time derivative of head at time $t = t_6$ given by Monte Carlo simulations

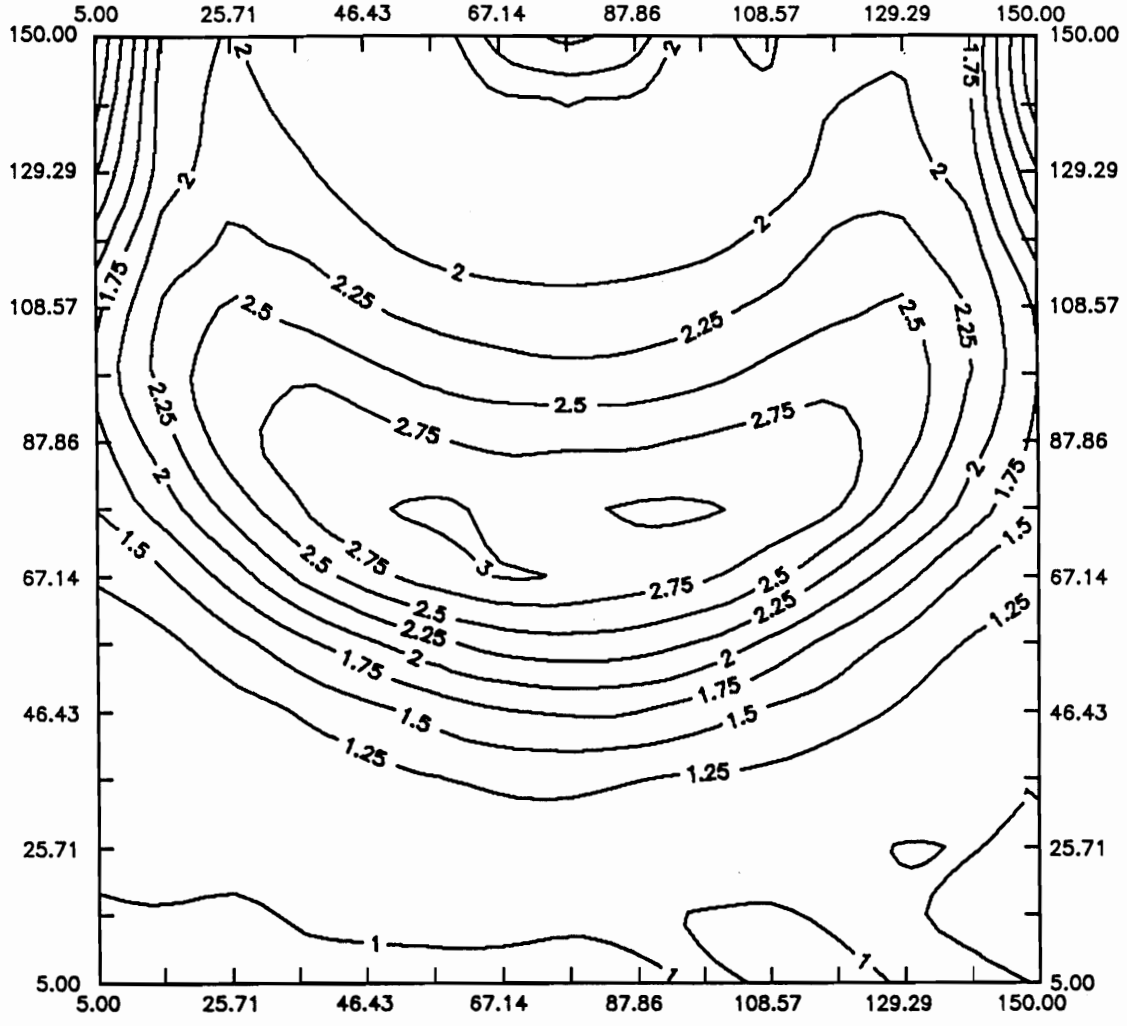


Figure 5.42 Contours of hydraulic gradient at time $t = t_6$ given by Monte Carlo simulations

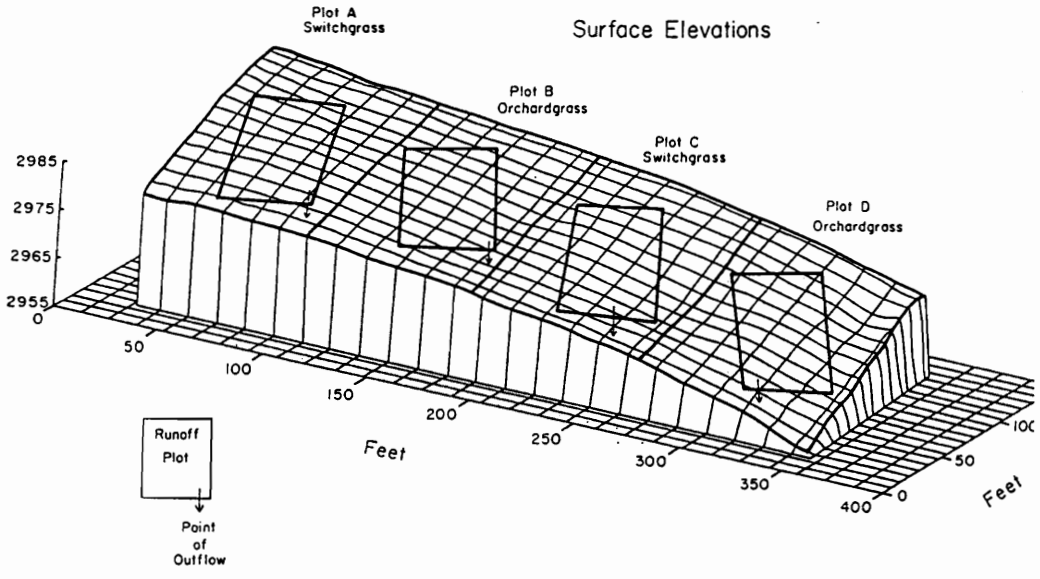


Figure 6.1 Geometries and surface elevations of Plot A at Beckley site

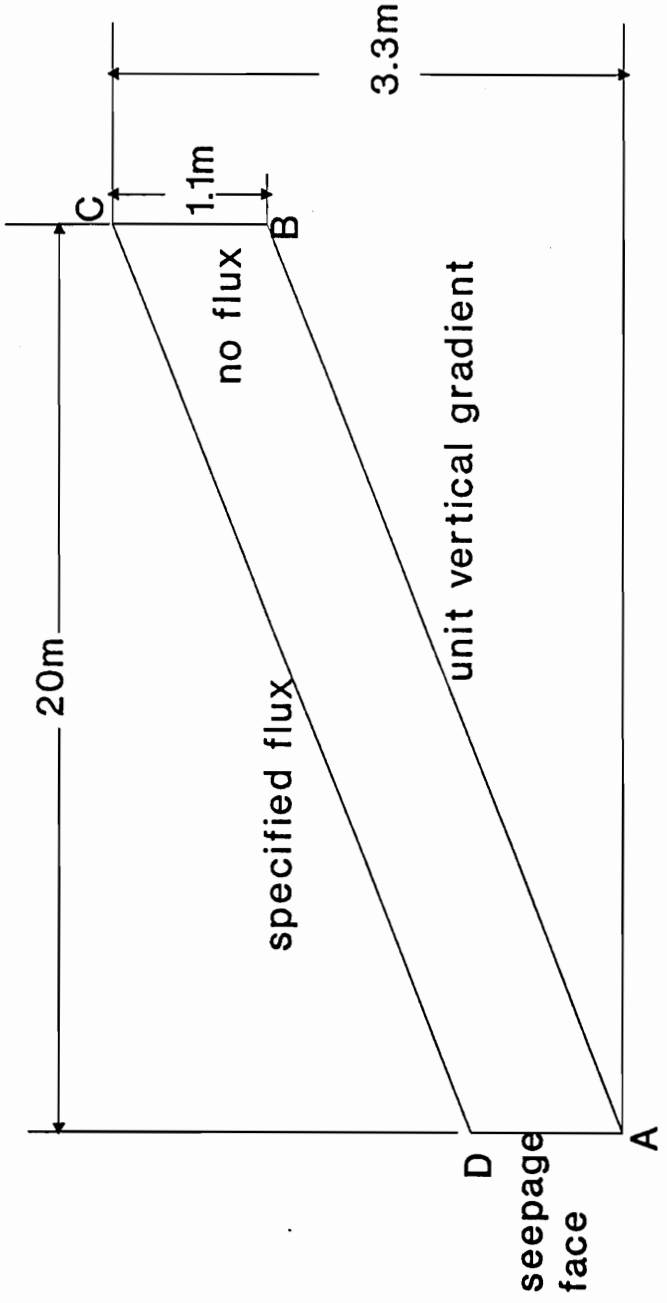


Figure 6.2 Geometries of the transect for simulation of a rainfall and subsurface runoff process at Beckley site

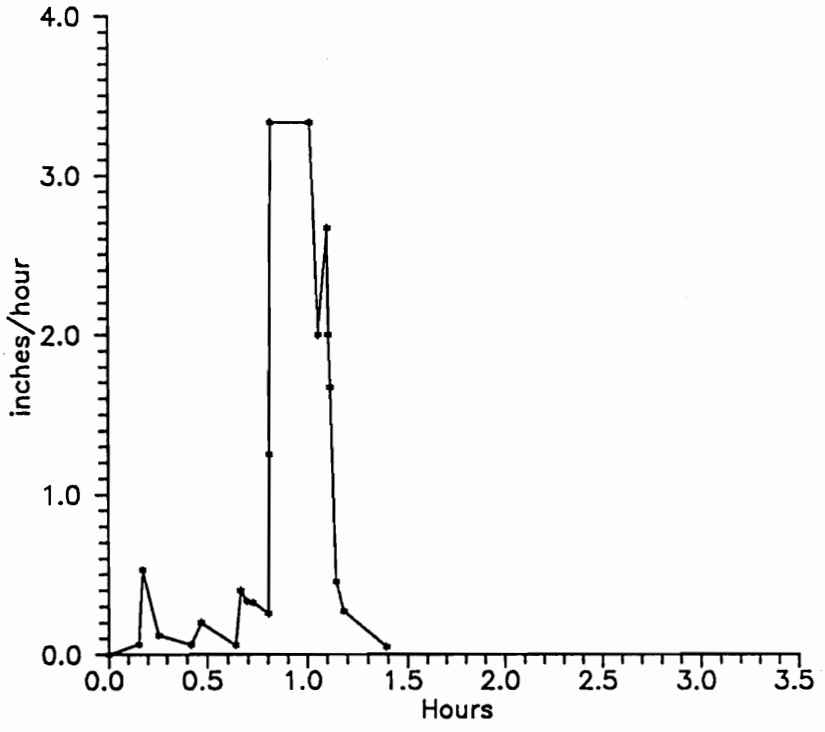


Figure 6.3 Rainfall data for Beckley site simulation

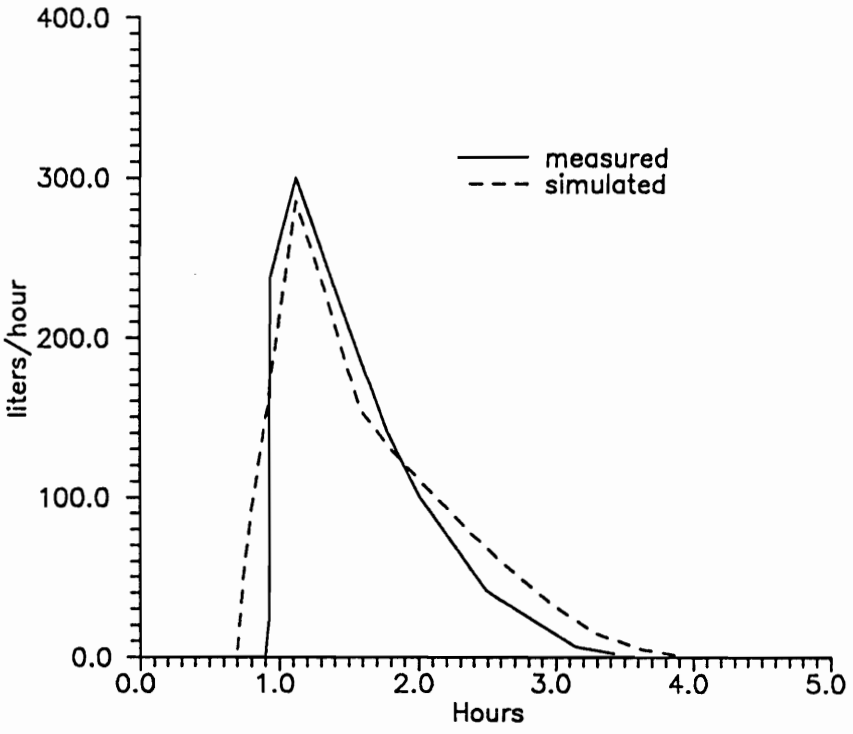


Figure 6.4 Comparison of subsurface runoff for Beckley site

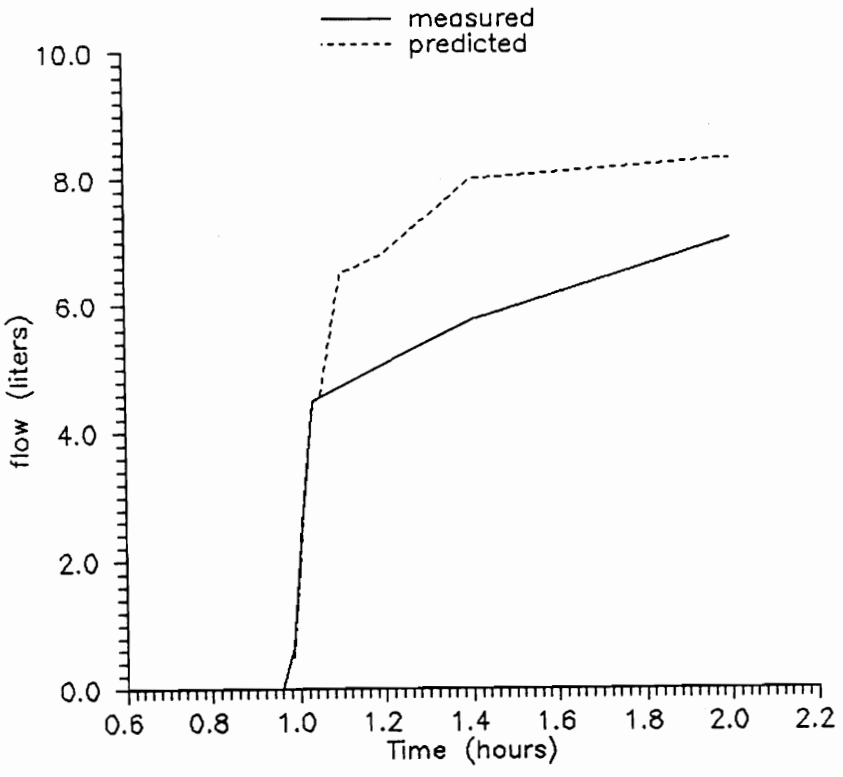


Figure 6.5 Comparison of cumulative surface runoff

Table 5.1 Statistics of soil properties for steady-state gravity flow simulations

| | Soil | $K_s(cm/hr)$ | $\alpha(cm^{-1})$ | $n$ |
|---|---|---|---|---|
| arith. mean | | 1.66 | 0.0228 | 1.31 |
| geo. mean | #1 | 1.51 | 0.0211 | 1.30 |
| arith. mean | | 0.41 | 0.0082 | 1.32 |
| geo. mean | #2 | 0.37 | 0.0073 | 1.32 |
| arith. mean | | 3.47 | 0.0210 | 1.77 |
| geo. mean | #3 | 2.81 | 0.0125 | 1.73 |

Table 5.2 Statistics of soil properties for areal source transient flow simulations

| | Parameter | Mean | Std Dev | Corr Length |
|---|---|---|---|---|
| Input | $\mu_{\ln(d)}$ | -5.5 | 0.20 | 4 blocks |
| | $\sigma_{\ln(d)}$ | 0.6 | 0.30 | 4 blocks |
| | $\theta_s$ | 0.4 | 0.02 | 4 blocks |
| Output | $\ln(\alpha)$ | -4.32 | 0.521 | 3.83 blcoks |
| | $\ln(n)$ | 0.58 | 0.074 | 3.44 blocks |
| | $\ln(K_s)$ | 1.07 | 0.310 | 3.84 blocks |

Table 5.3 Satistics of soil properties for point source infiltration simulation

| | Parameter | Mean | Std Dev | Corr Length |
|---|---|---|---|---|
| Input | $\mu_{\ln(d)}$ | -5.50 | 0.25 | 4 blocks |
| | $\sigma_{\ln(d)}$ | -0.50 | 0.25 | 4 blocks |
| | $\theta_s$ | 0.35 | 0.02 | 4 blocks |
| Output | $\ln(\alpha)$ | -4.59 | 0.389 | 3.67 blocks |
| | $\ln(n)$ | 0.57 | 0.040 | 3.24 blocks |
| | $\ln(K_s)$ | 1.08 | 0.416 | 3.65 blocks |

Table 6.1 Statistics of soil properties for simulation for Beckley site

Saturated Conductivity (in m/hour)

| | Measured | Estimated[1] |
|---|---|---|
| Geometric mean | 0.030 | 0.021 |
| Variance of $ln(K_s)$ | 2.340 | 1.750 |

[1] Using Equation 3.3

VG parameters calculated from PSD data

| | $\alpha$ ($m^{-1}$) | $n$ |
|---|---|---|
| geometric mean | 1.200 | 1.400 |
| variance | 0.385 | 0.128 |

Table 6.2 Initial Volumetric Soil Water Content, Plot A

| | Depth | | | |
|---|---|---|---|---|
| Tube No. | 20 cm | 40 cm | 60 cm | 80 cm |
| 1 | 42.6 | 43.7 | 40.5 | 36.4 |
| 2 | 42.8 | 43.8 | 43.2 | 44.5 |
| 3 | 41.9 | 43.5 | 43.7 | 42.5 |
| 4 | 42.2 | 44.3 | 36.2 | 41.0 |
| 5 | 43.5 | 47.1 | 46.8 | 40.2 |
| 6 | 41.5 | 40.8 | 38.2 | ---- |

# References


Ababou, R. and L. W. Gelhar, 1988. "A high resolution finite difference simulator for 3D unsaturated flow in heterogeneous media", *Computational Methods in Water Resources,* M.A. Celia *et al.* (eds), Elsvier, 1:173-178

Abramowitz, M. and I. A. Stegun, 1965. *Handbook of Mathematical Functions,* Dover Publications Inc., New York, 1045 pp

Anderson, J. and A. M. Shapiro, 1983. "Stochastic analysis of one-dimensional steady state unsaturated flow: A comparison of Monte Carlo and perturbation methods", *Water Resources Res.,* 19:121-133

Arya, L. M. and J. F. Paris, 1981. "A physico-empirical model to predict soil moisture characteristics from particle size distribution and bulk density data", *Soil Sci. Soc. Am. J.,* 45:1023-1030

Bathala, C. T., A. R. Rao and J. A. Spooner, 1980. "Linear system models for regional aquifer evaluation studies", *Water Resources Res.* 16:409-422

Binley, K. and R. Beven, 1989. "Unsaturated flow in heterogeneous hillslopes", *Water Resources Res.* 25:576-587

Bresler, E. and G. Dagan, 1983. "Unsaturated flow in spatially variable fields", *Water Resources Res.,* 19(2).

Brooks, R. H. and A. T. Corey, 1964. "Hydraulic properties of porous media", *Colorado State U., Hydrology Paper,* No. 3:27pp

Dagan, G. 1979. "Models of groundwater flow in statistically homogeneous porous formations", *Water Resources Res.* 15:47-63

Dettinger, M. D. and J. L. Wilson, 1981. "First order analysis of uncertainty in numerical models of groundwater flow, Part 1. Mathematical development", *Water Resources Res.* 17:149-161

El-Kadi, A. I.,1984. "Modeling variability in ground-water flow", *International Ground Water Modeling Center, GWMI 84-10,* Holcomb Res. Inst., Butler University, Indianapolis, Indiana

El-Kadi, A. and W. Brusaert, 1985. "Applicability of effective parameters for unsteady flow in nonuniform aquifers", *Water Resources Res.* 21:183-198

El-Kadi, A. I.,1987. "Variability of infiltration under uncertainty in unsaturated zone parameters", *Water Resources Res.* 21:587-596

Freeze, R. A. 1980. "A stochastic-conceptual analysis of one-dimensional groundwater flow in nonuniform homogeneous media", *Water Resources Res.* 11:725-741

Gutjahr, A. L., L. W. Gelhar, A. A. Bakr and J. R. MacMillan, 1978. "Stochastic analysis of spatial variability in subsurface flows, 2. Evaluation and application", *Water Resources Res.* 14:953-959

Gutjahr, A., P. Kallay and J. L. Wilson, 1987. "Stochastic models for two-phase flow - a spectral perturbation approach", *EOS, Trans. AGU,* 68:1266-1267

Hopmans, J. W., H. Schukking and P. J. J. F. Torfs, 1988. "Two-dimensional steady state unsaturated water flow in heterogeneous soils with autocorrelated soil properties", *Water Resources Res.*, 24:2005-2017

Haverkamp, R. and J.-Y. Parlange, 1986. "Predicting the water retention curve from particle size distribution: 1. Sandy soils without organic matter", *Soil Sci.,* 142:325-339

Jazwinski, A. H., 1970. *Stochastic Processes and Filtering Theory,* Academic, San Diego, Calif.

Journel, A. G. and Ch. J. Huijbregts, 1978. *Mining Geostatistics, Academic Press,* 600 p.

Kuo, C.Y., J. L. Zhu and L. A. Dollard, 1989. *A Study of Infiltration Trenches,* Virginia Water Resources Research Center, Bulletin 163

Luster, G. R. 1985. "Raw material for portland cement: Application of conditional simulation or coregionalization", *Ph.D dissertation, Stanford University,* Stanford, CA

Mantoglou, A. and L. W. Gelhar, 1987 a. "Stochastic modeling of large-scale transient unsaturated flow systems", *Water Resources Res.* 23:37-46

Mantoglou, A. and L. W. Gelhar, 1987 b. "Capillary tension head variance, mean soil moisture content and effective specific soil moisture capacity of transient unsaturated flow in stratified soils", *Water Resources Res.* 23:47-56

Mantoglou, A. and L. W. Gelhar, 1987 c. "Effective hydraulic conductivities of transient unsaturated flow in stratified soils", *Water Resources Res.* 23:57-67

Matern, B. 1986. *Spatial Statistics,* Lecture Notes in Statistics, 36, Springer Verlag, Berlin, 151pp.

Mualem, Y., 1984. "Prediction of the soil boundary wetting curve", *Soil Sci.* 127:379-390

Reddy, J. N., 1984. "An introduction to the finite element method", *McGraw-Hill Book Company,* 495pp

Russo, D. and E. Bresler, 1981. "Effect of field variability in soil hydraulic properties on solutions of unsaturated water and salt flows", *Soil Sci. Soc. America Journal,* 45(4):675-681

Smith, L. and R. A. Freeze, 1979. "Stochastic analysis of steady-state groundwater flow in a bounded domain, 2:Two-dimensional simulations", *Water Resources Res.,* 15:1543-1559

Schweppe, F. C., 1973. *Uncertain Dynamic Systems,* Prentice-Hall, Englewood, Cliffs, N.J.

van Genuchten, M. Th., 1980. "A close-form equation for predicting the hydraulic conductivity of unsaturated soils", *Soil Sci. Soc. Amer. J.,* 44:892-898

Warren, J. E. and H. S. Price, 1961. "Flow in heterogeneous porous media", *Society of Petroleum Engineers Journal* 1:153-169

Yeh, T.-C., L. W. Gelhar and A. L. Gutjahr, 1985 a. "Stochastic analysis of unsaturated flow in heterogeneous soils: 1. Statistically isotropic media", *Water Resources Res.* 21:447-456

Yeh, T.-C., L. W. Gelhar and A. L. Gutjahr, 1985 b. "Stochastic analysis of unsaturated flow in heterogeneous soils: 2. Statistically aniostripic media with variable alpha", *Water Resources Res.* 21:457-464

Yeh, T.-C., L. W. Gelhar and A. L. Gutjahr, 1985 c. "Stochastic analysis of unsaturated flow in heterogeneous soils: 3. Observations and applications", *Water Resources Res.* 21:465-471

# Vita

The author was born on December 17, 1959 in Jiangsu Province, China. He received BS degree in Mechanical Engineering in 1982 from Shandong Institute of Mining, China. He entered Virginia Tech in September, 1984 and received MS degree in Civil Engineering in December 1986.